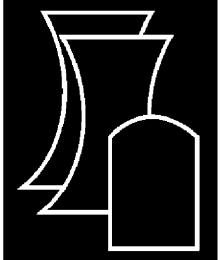

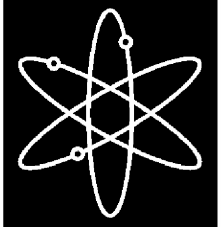

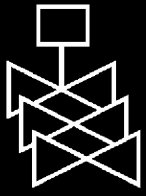

LA-UR-05-6146

Integrated Chemical Effects Test Project: Test #2 Data Report

Los Alamos National Laboratory

U.S. Nuclear Regulatory Commission
Office of Nuclear Regulatory Research
Washington, DC 20555-0001

LA-UR-05-6146

Integrated Chemical Effects Test Project: Test #2 Data Report

Manuscript Completed: August 2005
Date Published: September 2005

Principal Investigator: Jack Dallman

Prepared by
J. Dallman, B. Letellier, J. Garcia, M. Klasky,
W. Roesch, J. Madrid
Los Alamos National Laboratory
Los Alamos, NM 87545

K. Howe, D. Chen
University of New Mexico

B. P. Jain, NRC Project Manager

Prepared for
Division of Engineering Technology
Office of Nuclear Regulatory Research
U.S. Nuclear Regulatory Commission
Washington, DC 20555-0001

LA-UR-05-6146

INTEGRATED CHEMICAL EFFECTS TEST PROJECT: TEST #2 DATA REPORT

ABSTRACT

A 30-day test was conducted in the Integrated Chemical Effects Test (ICET) project test apparatus. The test simulated the chemical environment present inside a pressurized water reactor containment water pool after a loss-of-coolant-accident. The initial chemical environment contained 14.54 kg of boric acid and 0.663 g of lithium hydroxide (LiOH). Trisodium phosphate (3.786 kg), hydrochloric acid (211 mL), and additional boric acid (600 g) were added beginning at 30 minutes and lasting until 4 hours into the test. The test was conducted for 30 days at a constant temperature of 60°C (140°F). The materials tested within this environment included representative amounts of submerged and unsubmerged aluminum, copper, concrete, zinc, carbon steel, and insulation samples. Representative amounts of concrete dust and latent debris were also added to the test solution. Water was circulated through the bottom portion of the test chamber during the entire test to achieve representative flow rates over the submerged specimens. The test solution reached a pH of 7.3, and the test solution turbidity steadied out at approximately 1 NTU after 5 days. No precipitates were observed in the solution, but large amounts of white deposits (nominally 0.125 to 0.250 in. diam) were observed on the submerged galvanized steel, aluminum, and inorganic zinc coated steel coupons. The test solution remained clearly Newtonian for the entire test. Aluminum was not detectable in the solution. Calcium, magnesium, silica, and sodium were prevalent in the solution.

CONTENTS

LIST OF APPENDICES

LIST OF FIGURES

LIST OF TABLES

INTEGRATED CHEMICAL EFFECTS TEST PROJECT: TEST #2 DATA REPORT

EXECUTIVE SUMMARY

The U.S. Nuclear Regulatory Commission (NRC) Office of Nuclear Regulatory Research has developed a comprehensive research program to support resolution of Generic Safety Issue (GSI)-191. GSI-191 addresses the potential for debris accumulation on pressurized-water-reactor (PWR) sump screens with the consequent loss of emergency-core-cooling-system (ECCS) pump net-positive-suction-head margin. Among the GSI-191 research program tasks is the experimental investigation of chemical effects that may exacerbate sump-screen clogging.

The Integrated Chemical Effects Test (ICET) project represents a joint effort by the U.S. NRC and the nuclear utility industry, undertaken through the Memorandum of Understanding on Cooperative Nuclear Safety between NRC and EPRI (Electric Power Research Institute), Addendum on Integral Chemical Effects Testing for PWR ECCS Recirculation. The ICET project simulates the chemical environment present inside a containment water pool after a loss-of-coolant-accident and monitors the chemical system for an extended time to identify the presence, composition, and physical characteristics of chemical products that form during the test. The ICET test series is being conducted by Los Alamos National Laboratory at the University of New Mexico, with the assistance of professors and students in the civil engineering department.

This report describes the ICET experimental apparatus and surveys the principal findings of Test #2. As an interim data report compiled during preparation for subsequent ICET tests, this description summarizes both primary and representative findings that were available at the time the report was prepared. Additional analyses may be conducted by the NRC and the nuclear power industry to enhance the findings obtained from this test.

All of the ICET tests are being conducted in an environment that simulates expected containment pool conditions during recirculation. The initial chemical environment contains 2800 mg/L of boron, 100 mg/L of hydrochloric acid (HCl), and 0.7 mg/L of lithium hydroxide (LiOH). Tests are conducted for 30 days at a constant temperature of 60°C (140°F). The materials tested within this environment include representative amounts of submerged and unsubmerged aluminum, copper, concrete, zinc, carbon steel, and insulation samples. Representative amounts of concrete dust and latent debris are also added to the test solution. Tests consist of an initial 4-hour spray phase to simulate containment spray interaction with the unsubmerged samples. Water is circulated through the bottom portion of the test chamber during the entire test to achieve representative flow rates over the submerged specimens.

ICET Test #2 was conducted using trisodium phosphate (TSP) to control pH, with a target pH of 7. Insulation samples consisted of scaled amounts of NUKON™ fiberglass material. In addition, 373 metal coupon samples and one concrete sample were contained within the test apparatus. Process control consisted of monitoring online measurements of recirculation flow rate, test solution temperature, and pH. Flow rate and temperature were controlled to maintain the desired

values of 25 gpm and 140°F. Daily water samples were obtained to conduct pH, turbidity, total suspended solids, kinematic viscosity, and shear-dependent viscosity measurements and to conduct analytical laboratory evaluations of the chemical elements present. In addition, microscopic evaluations were conducted on water sample filtrates, fiberglass, coupons, sediment, and precipitated solids.

Before time zero, 14.54 kg of boric acid and 0.663 g of LiOH were dissolved in the ICET tank. The measured in-line probe pH was 4.3, which was the expected value obtained from analytical predictions. TSP Batch 1 (300 g boric acid, 1893 g TSP) and Batch 2 (300 g boric acid, 1893 g TSP, 211 mL of 12.29 N HCl**)** were metered into the recirculation line from 30 minutes until 4 hours into the test. Upon the addition of these prepared batches, the pH began to rise until it reached a pH of 7.32 (bench-top reading) 4 hours after the initiation of TSP addition. The test ran uninterrupted for 30 days, and the conditions were maintained within the required flow and temperature ranges.

Observations of the test solution indicated similar behavior of the solution both at room temperature and test temperature. No chemical byproducts were visible in the water, but large amounts of white deposits (nominally 0.125 to 0.250 in. diam) were observed on the submerged galvanized steel, aluminum, and inorganic zinc coated steel coupons.

Analyses of the test solution indicated that aluminum was not detectable in the solution. Calcium, magnesium, silica, and sodium were prevalent in the solution.

Examinations of fiberglass taken from the test apparatus after 15 days of testing indicated evidence of chemical products and a weblike material that spanned individual fibers. After 30 days of testing, the weblike material was more prevalent, and contiguous webbing appeared to span multiple fibers.

Daily measurements of the constant-shear kinematic viscosity revealed an approximately constant value at test temperature and room temperature for the unfiltered samples. Shear-dependent viscosity measurements indicated that the test solution at test temperature and room temperature was representative of Newtonian fluid.

The ICET test series is being conducted under an approved quality assurance (QA) program, and QA procedures and project instructions were reviewed and approved by the project sponsors. Analytical laboratory results are generated under a quality control program approved by the Environmental Protection Agency (EPA), and other laboratory analyses are performed using standard practices, as referenced in the body of this report.

ACKNOWLEDGMENTS

The principal authors of this report gratefully acknowledge the assistance of the following persons, without whom successful completion of ICET Test #2 could not have been accomplished. Mr. John Gisclon, representing the Electric Power Research Institute, again contributed much practical, timely advice on preparation of the QA experimental project instructions. Mr. Michael Niehaus from Sandia National Laboratories provided a characterization of time-dependent strain-rate viscosity measurements for the circulating solution. Mr. Luke Bartlein, of Los Alamos National Laboratory's Nuclear Design and Risk Analysis group (D-5), provided timely and accurate tagging of all test pictures and analytical images. Mr. Jim Young, of group PS-1, again provided valuable reviews and inputs to QA documentation and practices. The authors also express their gratitude for the contributions and continued participation of numerous NRC staff members who reviewed the project instructions and preliminary data to ensure relevance to plant safety, high-quality defensible results, and timely execution of this test. Dr. Rob Tregoning, in particular, provided valuable suggestions on data analyses and detailed review comments on the report.

The authors acknowledge Ms. Eileen Patterson of IM-1, Los Alamos National Laboratory, and Ms. Katsura Fujiike, OMICRON, for their editing support.

Finally, the authors thank Mr. Louis Archuleta and Dr. Frank Sciacca, of OMICRON, for their efforts in consolidating the various inputs of text, test data, and laboratory analyses into a cohesive document.

ACRONYMS AND ABBREVIATIONS

Al	Aluminum
Au	Gold
CPVC	Chlorinated Polyvinyl Chloride
CS	Coated steel
Cu	Copper
DAS	Data Acquisition System
DHR	Decay Heat Removal
ECCS	Emergency Core-Cooling System
EDS	Energy-Dispersive Spectroscopy
EPA	Environmental Protection Agency
EPRI	Electric Power Research Institute
ESEM	Environmental Scanning Electron Microscopy
F	Filtered
GS	Galvanized Steel
GSI	Generic Safety Issue
HCl	Hydrochloric Acid
ICET	Integrated Chemical Effects Tests
ICP	Inductively Coupled Plasma
ICP-AES	Inductively Coupled Plasma – Atomic Emission Spectroscopy
IOZ	Inorganic Zinc
LANL	Los Alamos National Laboratory
LiOH	Lithium Hydroxide
LOCA	Loss-of-Coolant Accident
NIST	National Institute of Standards and Technology
NRC	Nuclear Regulatory Commission
NTU	Nephelometric Turbidity Unit
Pd	Palladium
PI	Project Instruction
PVC	Polyvinyl Chloride
PWR	Pressurized Water Reactor
QA	Quality Assurance
QC	Quality Control
RO	Reverse Osmosis

SEM	Scanning Electron Microscopy
SS	Stainless Steel
T1	ICET Test #1
T2	ICET Test #2
TEM	Transmission Electron Microscopy
TOC	Total Organic Carbon
TSP	Trisodium Phosphate
TSS	Total Suspended Solid
U	Unfiltered
UNM	University of New Mexico
US	Uncoated steel
U.S.	United States
WD	Working Distance
XRD	X-Ray Diffraction
XRF	X-Ray Fluorescence

This page is intentionally blank.

1 INTRODUCTION

The Integrated Chemical Effects Test (ICET) project represents a joint effort by the United States (U.S.) Nuclear Regulatory Commission (NRC) and the nuclear utility industry to simulate the chemical environment present inside a containment structure after a loss-of-coolant accident (LOCA) and to monitor the chemical system for an extended time to identify the presence, composition, and physical characteristics of chemical products that may form. Among the many secondary objectives (not addressed by the ICET project), should products of this nature be found during the ICET series, are determining the cause and potential quantity of the products and characterizing their head-loss properties in combination with fibrous debris. The ICET test series is being conducted by Los Alamos National Laboratory (LANL) at the University of New Mexico (UNM), with the assistance of professors and students in the civil engineering department.

This report surveys the principal findings of ICET Test #2. Test #2 was initiated on February 5, 2005, and was terminated on March 7, 2005. As an interim data report compiled during preparation for subsequent ICET tests, this report summarizes both primary and representative findings, but it cannot be considered comprehensive. For example, only a small selection out of several hundred photographs is presented here. In addition, this report focuses on the presentation of observations and data without in-depth analyses or interpretations. Observed trends and typical behaviors are noted. Section 2 of this report presents more thoroughly the objectives and background of the ICET test series. Section 3 briefly describes the experimental apparatus and test articles/samples, the analytical methods used to characterize samples, and the quality assurance (QA) process that governs the performance of these tests. Section 4 presents key results in both graphical and narrative form. Section 5 presents a summary of the key findings made during Test #2.

2 BACKGROUND AND OBJECTIVE

Containment buildings of pressurized-water reactors (PWRs) are designed to accommodate the energy release following a postulated accident. They also permit recirculation of reactor coolant and emergency-core-cooling-system (ECCS) water to the decay heat removal (DHR) heat exchangers. The water collected in the sump from the reactor coolant system, the safety injection system, and the containment spray system is recirculated to the reactor core to remove residual heat. The sump contains a screen to protect system structures and components in the containment spray and ECCS flow paths from the effects of debris that could be transported to the sump. Concerns have been raised that fibrous insulation material could form a mat on the screen, which would obstruct flow, and that chemical reaction products such as gelatinous or crystalline precipitates could migrate to the screen, causing further blockage and increased pressure-head losses across the debris bed. Other adverse chemical effects include the possibility of increased bulk fluid viscosity that also would increase flow losses through a debris bed.

The ICET test series was conceived as a limited-scope suite of five tests containing different constituents, with each test lasting between 15 and 30 days. An industry-prepared test plan (Ref. 1) provided the rationale for the selection of test conditions. The ICET apparatus was designed and constructed to meet the functional requirements of the test plan. Briefly, the ICET apparatus consists of a large stainless-steel (SS) tank with heating elements, spray nozzles, and associated recirculation pump and piping to simulate the post-LOCA chemical environment. Samples of metals, concrete, and insulation debris are scaled in proportion to their relative surface areas found in containment and in proportion to a maximum test dilution volume of 250 gal. of circulating fluid. Representative chemical additives, temperature, and material combinations are established in each test; the system then is monitored while corrosion and mixing occur for a duration comparable to the ECCS recirculation mission time.

The primary objectives for the ICET test series are to (1) determine, characterize, and quantify chemical reaction products that may develop in the containment sump under a representative post-LOCA environment, and (2) determine and quantify any gelatinous material that could be produced during the post-LOCA recirculation phase. For the purpose of this report, the term “gelatinous material” generically refers to any observed sample constituent with amorphous, hydrated, or noncrystalline physical characteristics. This adjective is sufficient to distinguish a material from chemical products that are crystalline in nature, but it is not intended to imply any specific head-loss behavior. The ICET series is not designed to test the head-loss characteristics of chemical products that might be observed.

This is the second report in the ICET test series. The first report—Integrated Chemical Effects Test Project: Test #1 Data Report—was published in June 2005 (Ref. 2).

3 EXPERIMENTAL MATERIALS AND METHODS

The functional description and physical attributes of the ICET test apparatus were presented in detail in the ICET Test #1 data report (Ref. 2). The experimental apparatus is briefly described below. The following discussions also present the ICET experimental plan and test matrix to provide context for the results of Test #2, the analytical methods that were applied for daily monitoring and sample analysis, and the QA approach that is being followed during execution of the ICET series.

3.1 Chemical Test Apparatus Functional Description

The test apparatus was designed to meet the functional requirements of the Project Test Plan (Ref. 1). Important functional aspects of the test apparatus are as follows:

1. The central component of the system is a test tank. The test apparatus was designed to preclude solids from settling in the test piping.
2. The test tank is capable of maintaining both a liquid and a vapor environment, as would be expected in post-LOCA containment.
3. The test loop is capable of controlling the liquid temperature at 140°F (±5°F).
4. The system is capable of circulating water at flow rates that simulate spray flow rates per unit area of containment cross section.
5. The test tank provides for water flow over submerged test coupons that is representative of containment pool fluid velocities expected at plants.
6. Piping and related isolation valves are provided such that a section of piping can be isolated without interrupting the test.
7. The pump discharge line is split in two: one branch is directed to the spray header located in the vapor space inside the tank; the other branch returns to the liquid side of the tank. Each branch is provided with an isolation valve and the spray line includes a flow meter.
8. A flow meter is provided in the recirculation piping.
9. The pump circulation flow rate is controlled at the pump discharge to be within ±5% of the flow required to simulate fluid velocities in the tank. Flow is controlled manually.
10. The tank accommodates a rack of immersed sample coupons, including the potential reaction constituents identified in the test plan.
11. The tank also accommodates six racks of sample coupons that are exposed to a spray of liquid that simulates the chemistry of a containment spray system. Provision is made for visual inspection of these racks.
12. The coupon racks provide sufficient space between the test coupons to preclude galvanic interactions among the coupons. The different metallic test coupons are electrically isolated from each other and the test stand to prevent galvanic effects

resulting from metal-to-metal contact between specimens or between the test tank and the specimens.

13. The fluid volumes and sample surface areas are based on scaling considerations that relate the test conditions to actual plant conditions.
14. All components of the test loop are made of corrosion-resistant material (for example, SS for metallic components).

The as-built test loop consists of a test tank, a recirculation pump, 2 flow meters, 10 isolation valves, and pipes for connecting the major components, as shown schematically in Figure 3-1.

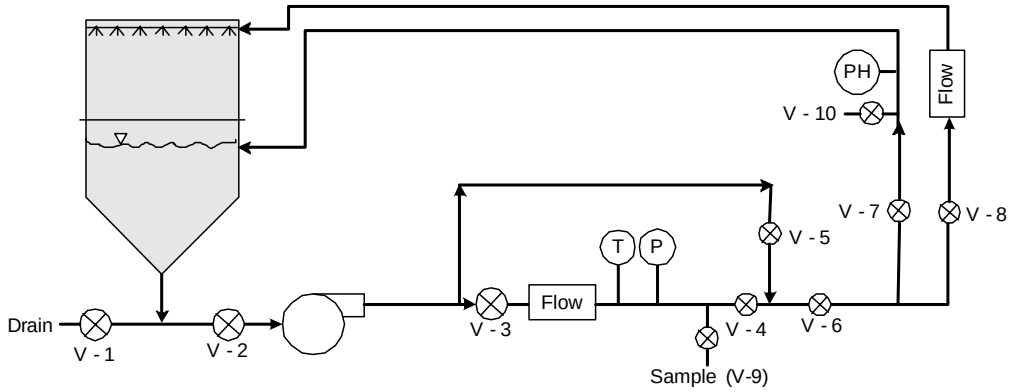

Figure 3-1. Test loop process flow diagram.

3.2 Experiment Plan and Test Matrix

ICET test parameters were selected based on literature surveys and the results of surveys of U.S. nuclear power plants. Quantities of test materials were selected to preserve the scaling of representative ratios between material surface areas and total cooling-water volumes. Chemical additives also simulate the post-LOCA sump environment. The Project Test Plan (Ref. 1) is the basis for the following information in this section.

The materials included in the tests are zinc, aluminum, copper, carbon steel, concrete, and insulation materials such as fiberglass and calcium silicate. The amounts of each material are given in Table 3-1 in the form of material-surface-area to water-volume ratios, with the exceptions of concrete dust, which is presented as a mass-to-water-volume ratio, and fiberglass and calcium silicate, which are presented as insulation-volume-to-water-volume ratios. Also shown in the table are the percentages of the materials that are submerged and unsubmerged in the test chamber.

Table 3-1. Material Quantity/Sump Water Volume Ratios for the ICET Tests

Material	Value of Ratio for the Test (ratio units)	Percentage of Material Submerged (%)	Percentage of Material Unsubmerged (%)
Zinc in Galvanized Steel	8.0 (ft^2/ft^3)	5	95
Inorganic Zinc Primer Coating (non–top coated)	4.6 (ft^2/ft^3)	4	96
Inorganic Zinc Primer Coating (top coated)	0.0 (ft^2/ft^3)	–	–
Aluminum	3.5 (ft^2/ft^3)	5	95
Copper (including Cu-Ni alloys)	6.0 (ft^2/ft^3)	25	75
Carbon Steel	0.15 (ft^2/ft^3)	34	66
Concrete (surface)	0.045 (ft^2/ft^3)	34	66
Concrete (particulate)	0.0014 (lbm/ft^3)	100	0
Insulation Material (fiberglass or calcium silicate)	0.137 (ft^3/ft^3)	75	25

The physical and chemical test parameters which are critical for defining the tank environment and which have a significant effect on sump-flow blockage potential and gel formation are identified in Reference 1. These physical and chemical parameters are summarized as follows:

Physical Parameters

• Volume in the test tank	949 L	(250 gal.)
• Circulation flow	0–200 L/min	(0–50 gpm)
• Spray flow	0–20 L/min	(0–5 gpm)
• Sump temperature	60°C	(140°F)

Chemistry Parameters

• H_3BO_3 concentration	2800 mg/L as boron
• $Na_3PO_4 \cdot 12H_2O$ concentration	As required to reach pH 7 in the simulated sump fluid
• NaOH concentration	As required to reach pH 10 in the simulated sump fluid
• HCl concentration	100 mg/L
• LiOH concentration	0.7 mg/L as Li

The parameters planned for each ICET test run are described in Table 3-2.

Table 3-2. Test Series Parameters

Run	Temp	TSP	NaOH	pH	Boron	Note
	(°C)	$Na_3PO_4 \cdot 12H_2O$			**(ppm)**	
1	60	N/A	Yes	10	2800	100% fiberglass insulation test. High pH, NaOH concentration, as required by pH.
2	60	Yes	N/A	7	2800	100% fiberglass insulation test. Low pH, TSP concentration, as required by pH.
3	60	N/A	Yes	10	2800	80% calcium silicate/20% fiberglass insulation test. High pH, NaOH concentration, as required by pH.
4	60	Yes	N/A	7	2800	80% calcium silicate/20% fiberglass insulation test. Low pH, TSP concentration, as required by pH.
5	60	TBD	TBD	TBD	TBD	Confirmatory test; one of the above four tests will be repeated.

Note

The parameters in Table 3-2 are those presented in Reference 1 and were active when Test #2 was conducted. Subsequent revisions of Reference 1 reversed the order of Tests #3 and #4.

3.3 Data Compilation and Nomenclature

This section provides a brief guide to assist in accessing and interpreting the ICET Test #2 information and data presented in the following sections and in the appendices. Standardized nomenclature is defined first to clarify the origin of samples that are described in the data sets. The appendices are listed next along with a description of data compilation methods.

3.3.1 Nomenclature

Many spatially unique but physically similar sample types were collected in ICET Test #2. To ensure that consistent interpretations and comparisons of data sets are made, it is imperative that a standardized nomenclature be adopted when referring to each sample type. Many different qualitative descriptions of these samples might be equally suitable, but different adjectives convey different connotations to each observer. Therefore, the following definitions establish the convention used in this report when making generic references to sample type. Every effort should be made to adhere to this standard when interpreting the data so that all future audiences will have a common understanding of sample origins from the ICET series.

White Precipitate — The behavior of test solution at temperature and upon cooling is observed during testing. Precipitates and their prominence indicate chemical interactions occurring in the solution. White precipitate formed in Test #1 (T1) water solution samples drawn from the test loop. Upon cooling below the test temperature, T1 daily water samples extracted from the tank formed a visible white material that is referred to as a precipitate. This precipitate was absent in Test #2 (T2) water samples. One probable cause of the differences are the pH levels of the test solutions and their effects on aluminum samples. T1 had a high pH of about 9.5, whereas for T2 the pH was about 7.4. Aluminum solubility is highly dependent on pH levels. There may be other causes that effect the corrosion of aluminum and cause precipitates to form.

Latent Debris — Commercial power plant containments gradually accumulate dust, dirt, and fibrous lint that are generically referred to as latent debris. This classification distinguishes resident material from debris generated during the accident scenario. At the beginning of T2, measured quantities of crushed concrete and soil were added to simulate the latent debris present in containment. These materials were examined via scanning electron microscopy and energy dispersive spectroscopy (SEM/EDS) to establish a baseline composition for comparison to sediment samples (see “Sediment” below).

Sediment — Surrogate latent debris particulates and fugitive fiberglass fragments that were initially suspended in water at the beginning of T2 gradually settled to the bottom of the tank to form a layer of sediment. During the course of the test, additional material may have been deposited in this layer. At the conclusion of the test, the sediment layer was recovered as completely as possible.

White Residue — At the conclusion of Test #2, all water was drained slowly from the tank. Exposed metal surfaces that cooled rapidly collected a thin deposit of white residue or scale. Some of this material was scraped from internal piping surfaces and tank walls for comparison with other sample types. A similar residue was observed after Test #1.

Fiberglass — One of the principal debris types introduced to T2 was shredded fiberglass insulation. This debris was bundled in 3-in.-thick bags (or blankets) made of SS mesh to prevent ingestion through the pump and to better control the placement of fiberglass in various flow regimes. Fiberglass samples are designated by their placement in high-flow and low-flow areas of the tank. Additional, small, 4-in.-square envelopes of fiberglass were also prepared for

	extraction during the course of the test. These samples are referred to as “sacrificial” samples. One sample, called the “birdcage,” was constructed so that the fiberglass contained within was loose and not compacted. The birdcage fiberglass sat on the tank bottom and was removed on Day 30. Some amount of fiber, especially short fiber fragments, escaped the mesh bags and was deposited in other locations within the tank. This material is referred to as “fugitive” fiberglass.
Drain Screen	A 12-in.-tall screen made of coarse SS mesh (1/8-in. holes) wrapped into a 2-in.-diam cylinder was inserted into the outlet drain at the bottom of the tank to protect the pump from ingestion of large debris items. Two inches of the screen were inserted into the tank outlet to provide a solid base and stability. A 6-in.-tall drain collar was installed around the drain screen. This drain collar was a cylinder of fiberglass held in SS mesh. The drain collar was exposed to higher-velocity water flow than other samples in the tank. The drain collar fiberglass was examined as a separate debris location to identify any apparent differences with other sample locations.
Gelatinous Material	This term generically refers to any observed sample constituent with amorphous, hydrated, or noncrystalline physical characteristics.
Water Sample	Daily water samples are extracted from the ICET tank for elemental concentration analyses and physical property characterization. After properly flushing the sample line, some of the test solution is extracted directly from the tap. An equal amount of water is also generally collected through a micropore filter. Thus, daily water samples are designated as filtered (F) and unfiltered (U), and a corresponding filter paper exists in the sample archive for each daily sample that is collected.
High-Volume Filter	In addition to the relatively small volumes collected during daily water sampling, larger quantities were periodically extracted for filtration to determine whether suspended chemical products were present in the test liquid under in situ conditions. The intent of this exercise was to maintain the liquid temperature while forcing the liquid through a micropore filter under vacuum. Temperature control for the T2 high-volume filter samples was not ideal, so the collected filtrate may show evidence of temperature-dependent precipitation similar to that described for white precipitate in Test #1.

Filter Paper	Many different samples of tank solution were fractionated by micropore filtration into a liquid supernate and a solid filtrate that existed at the time and temperature conditions of the filtering process. These samples include (1) daily water samples filtered during extraction, (2) daily water samples filtered after cooling to room temperature, and (3) high-volume water samples.
Chemical Deposits	Sacrificial fiberglass samples that were extracted at Day 4, Day 15, and Day 30 showed evidence of chemical products forming on and between fiber strands. These products are referred to as "deposits," although the exact physical mechanism of formation is not well understood. The physical appearance suggests growth, agglomeration, or crystallization on and around the fiber strands over time rather than capture or impaction of particles from the bulk solution. This observation is supported by the fact that the small sacrificial fiberglass samples were located in a region of lower-velocity directed water flow (i.e., in the interior of larger blankets).
Concrete Sample	Several concrete chips (1/4– 3/4 in. diameter) were broken from the primary slab of submerged concrete and introduced to the tank in a small SS envelope at the start of the test. Examinations of these chips were conducted to determine if concrete surfaces provide a preferential site for gel formation.

Although these terms have been defined, the reader may note minor inconsistencies in the caption labels used in this document. The caption labels use the same descriptions that were recorded in laboratory notebooks to improve traceability of the data.

3.3.2 Usage

Eleven appendices are provided to present data collected for the sample types and analysis methods listed below. In addition, an appendix is provided with pertinent Test #2 project instructions.

A	SEM/EDS Data for Test #2, Day 15, High-Volume Filter
B	SEM/EDS Data for Test #2, Day 30, Corrosion Products
C	SEM/EDS Data for Unused and Test #2, Day 30, Coupons
D	ESEM and SEM/EDS Data for Test #2, Day 16 and Day 30, Fiberglass
E	SEM/EDS Data for Test #2, Day 30, Sediment
F	TEM Data for Test #2 Solution Samples
G	Test #2 Total Organic Carbon (TOC) Concentration
H	UV Absorbance Spectrum – Day 30 Solution Sample
I	XRD and XRF Data for Test #2, Day 30, Sediment and Fiberglass

J ESEM and SEM/EDS Data for Test #2, Day 4, Filtrate and Fiberglass Samples

K ICET Test #2: Pre-Test, Test, and Post-Test Project Instructions

The data in these appendices are largely qualitative in nature, consisting primarily of environmental scanning electron microscopy (ESEM), SEM, transmission electron microscopy (TEM) micrographs, and EDS spectra. Each appendix represents a separate session of laboratory work that can be traced to a batch of samples that were processed in chronological order. This organizational scheme preserves the connection with laboratory notebooks and timelines that naturally developed during operation; however, in a few cases, results for a given sample type may be mixed across two or more appendices because of the order in which the individual samples were analyzed.

ESEM analyses were added to the ICET diagnostic suite for the first time during Test #2 as a means of examining hydrated chemical products. This equipment operates as an electron microscope, but it does not require a high-vacuum condition in the sample chamber. Thus, a sample need only be thoroughly drained of free water content before examination rather than fully desiccated, making the ESEM ideal for examinations of biological and environmental specimens. The complementary EDS capability that is often found with equipment of this type is not presently functional at UNM, so duplicate examinations are often performed on the same ICET sample using ESEM to obtain images of hydrated structural details and SEM/EDS to obtain representative elemental compositions. Throughout the report, ESEM analyses are also indicated by the descriptions of “hydrated” and “low-vacuum” findings.

Transcriptions of the logbooks are provided for each appendix to better document commonalities that existed among the samples at the time of analysis. Interpretation and understanding of the images and their accompanying EDS spectra will be greatly improved by referring frequently to the logbook sample descriptions and sequences. Typically, a relatively large quantity of a test sample was delivered for SEM or TEM analysis, and then several small sub-samples were extracted for examination. Note that each sub-sample was assigned a sequential reference number during the laboratory session. These reference numbers have been cited in the figure captions whenever possible to preserve the connection between the micrographs and the notebook descriptions. Electronic filenames have also been stamped on the images to permit retrieval of the original data files that are archived elsewhere. Individual data sets for a given sample item have been collated into a typical sequence of (1) visual image, (2) EDS spectra, and (3) semi-quantitative mass composition.

For most of the EDS spectra, semi-quantitative mass compositions are also presented. These results are obtained from a commercial algorithm that decomposes the spectra into the separate contributions of each element. Several caveats should be considered when interpreting the numeric compositions thus obtained; however, despite these caveats, semi-quantitative EDS analysis offers a natural complement to micrographic examination as a survey technique for identifying trends in composition.

1. The spectral deconvolution algorithm is based on a library of unique signatures of each element that were obtained for pure samples using a standard beam setting that may not identically match the conditions applied for the test item.
2. The operator must select a limited number of elements to be used in the proportional mass balance. These candidates are chosen from among the peaks that are observed in the spectrum; however, the composition percentages can vary, depending on which elements are included in the list. In a few cases, two or more alternative compositions have been generated by selecting a different set of elements from the same spectrum to illustrate the sensitivity of this technique to operator input.
3. The spectral unfolding algorithm is a statistical technique having a precision that depends on the relative quality of the data in each peak. Compositions with high R^2 correlation coefficients and total-mass normalization factors closer to unity represent the more-reliable estimates. The precision obtained in the fit depends on the duration of the scan and the number of counts received in each energy bin.
4. All sub-samples examined in the SEM microprobe facility are coated with a thin layer of either carbon or gold/palladium alloy to prevent charge accumulation from the impinging electron beam. Spectral peaks visible for gold (Au) and palladium (Pd) are not indigenous to the samples.
5. The EDS spectral analysis software contains a peak-recognition algorithm and an automated cursor that snaps across the spectrum to locate each peak. An accompanying library of elemental energy signatures is also provided to suggest what constituents might be contributing to a given energy bin, but the operator must judge what label to assign to the spectral image. It is possible that some peaks near closely neighboring elements have been mislabeled in these images. However, every effort was made to choose from candidate elements that were most likely to be present in the test material. In a few cases, the spectral peaks were not labeled by the SEM operator. These spectra should be viewed as corroborating evidence for similar samples that are definitively labeled. Careful comparisons of the energy scales in combination with a library of electron-scattering energies can also be used to infer the origin of the more-prominent peaks that are present in unlabeled spectra.
6. Unless an obvious spatial heterogeneity is being examined, the exact location of an EDS spectrum is not always relevant because the operator chooses arbitrary sites that are visually judged to be representative. It is not possible to sample a surface comprehensively on a microscopic basis and compute average compositions. In many cases, two or three replicate spectra are provided for this purpose, but SEM/EDS is most effective as a survey diagnostic.
7. For several reasons, EDS analysis is not particularly sensitive to the presence of boron: (a) boron has a low atomic mass that does not interact well with electrons in the beam, (b) the emission lines are very close to those of carbon, and (c) the beam port material has a high absorption cross section for these emission energies. Therefore, the correction factors used in the semi-quantitative

composition analysis are quite large, as are the uncertainties in the estimated percentage of total composition for this element. There may be spectra presented in the appendices in which the lowest energy peak is labeled as either B or C, when in fact either both elements are present or the opposite element is present.

EDS locations were chosen manually at regions of specific interest. In many cases, multiple spectra were collected from a single sample and an annotated image is provided to identify the specific location. These annotated images are not generally identified in the laboratory logbook entries, but they are located within the relevant image cluster within the appendices.

Appendix F presents transmission electron microscopy data for water samples extracted from the ICET solution at Day 4, Day 15, and Day 30, respectively. The purpose of this examination was to determine whether the physical structure of any suspended products exhibits crystalline or amorphous characteristics. These data are also qualitative in nature, consisting generally of a set of high-resolution micrographs followed by companion electron diffraction images. The TEM sample holder consists of a carbon grid that is "lacey," or filamentary, in nature. This grid is visible as a relatively large-scale structure in the background of most images. Surface tension in a droplet of liquid suspends the particulates of interest across the grid so that the electron beam can illuminate the sample through the holes without interference from a substrate. Crystalline material will exhibit diffraction patterns unique to the molecular arrangement. Amorphous material that is diffuse or disorganized in structure will not exhibit regular diffraction patterns that can be identified.

Water samples submitted for TEM analysis are not temperature controlled because the temperature cannot be maintained during the examination.

In a few cases, data file names that were noted by the operator in the laboratory log were not successfully saved in electronic form. These cases are noted in the transcribed log sheets, but the corresponding images are unavailable and therefore not presented in the data sequence.

3.4 Analytical Methods

Data collected during Test #2 include the on-line measurements of temperature, pH, and loop flow rate. During the water grab sample analysis, bench-top measurements are obtained for temperature, pH, turbidity, total suspended solids (TSSs), and kinematic viscosity. The concentration of hydrogen in the tank atmosphere is also measured and can be used as an indicator of chemical reactions taking place. Water, fiberglass, and metal samples are taken to other laboratory locations for additional analyses. These analyses include strain-rate viscosity, SEM, EDS, TEM, inductively coupled plasma atomic emission spectroscopy (ICP-AES), x-ray fluorescence (XRF), and x-ray diffraction (XRD). Descriptions of the principles of operation and limitations of these analytical methods were provided in the Test #1 data report (Ref. 2).

3.5 Quality Assurance (QA) Program

A project QA manual was developed to satisfy the contractual requirements that apply to the ICET project. Specifically, those requirements were to maintain an appropriate level of QA in the areas of test loop design, sampling, chemicals, operation, and analysis to provide for credible results. These requirements were summarized in the contract requirement that QA was to be consistent with the intent of the appropriate sections of 10CFR50, Appendix B.

The 18 criteria of 10CFR50, Appendix B, were addressed separately in the QA manual, and the extents to which they apply to the ICET project were delineated. A resultant set of QA procedures was developed. In addition, project-specific instructions were written to address specific operational topics that required detailed step-by-step guidance. Project instructions (PIs) generally applicable to all tests were written for the following topics, and were followed for Test #2:

- Data Acquisition System (DAS)
- Coupon Receipt, Preparation, Inspection, and Storage
- DAS Alarm Response
- Transmission Electron Microscope Examination of Test Samples
- Scanning Electron Microscope Characterization of Test Samples
- Viscosity Measurements

Project instructions specific to Test #2 were written for the following:

- Pre-test Operations
- Chemical Sampling and Analysis
- Test Operations, Test #2 (TSP at pH = 7)
- Post-test Operations

The pre-test, test, and post-test operations PIs are included in Appendix K.

3.6 Test Loop Preparation

In preparation for Test #2, the experiment test loop was thoroughly cleaned to remove all deposits and residues associated with ICET Test #1. In addition to visual inspections, the test apparatus was flushed and cleaned per the written direction given in the pre-test operations PI (Ref. 3). The general procedure was to flush the system with ammonium hydroxide and then ethanol until it was visually clean and the water conductivity was less than 50 μS/cm.

3.7 Test Coupons and Samples

Each ICET experiment exposes metallic and concrete coupons to anticipated post-LOCA environments. Each coupon is approximately 12 in. square. The metallic coupons are

approximately 1/16 in. thick, except for the inorganic-coated steel coupons, which are approximately 3/32 in. thick. The concrete coupons (one per test) are approximately 1-1/2 in. thick.

Insulation materials are also exposed. For Test #2, fiberglass insulation samples were included in the test.

As with Test #1, Test #2 subjected seven racks of coupons to the specified environment, with one being submerged below the surface of the water level in the test tank and the remaining six held in the gas/vapor space of the tank. The number of coupons of each type employed in Test #2 was as follows:

Material	No. of Coupons
Coated Steel (CS)	77
Aluminum (Al)	59
Galvanized Steel (GS)	134
Copper (Cu)	100
Uncoated Steel (US)	3
Concrete	1

Note: Inorganic zinc (IOZ) coated steel and CS are the same coupon type.

The arrangement of the coupon racks in the test tank is schematically illustrated in Figure 3-2. The figure shows a side view of the ICET tank, with the ends of the seven CPVC racks illustrated. The normal water level is shown with the blue line in the figure. Rack #1 is the only submerged rack, and it sits on angle iron. It is centered in the tank, so that flow from the two headers reaches it equally. Racks #2–#4 are positioned above the water line, supported by angle iron in the tank. Racks #5-#7 are positioned at a higher level, also supported by angle iron. Racks #2-#7 are exposed to spray. In the figure, north is to the right, and south is to the left. Directions are used only to identify such things as rack locations and sediment locations.

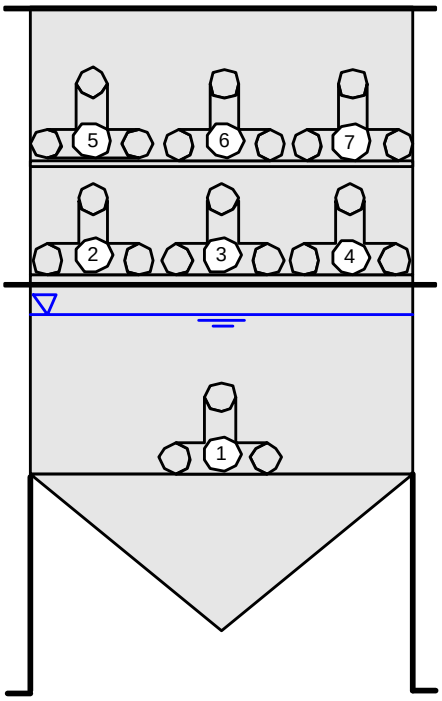

Figure 3-2. Coupon rack configuration in the ICET tank.

The configuration of an unsubmerged coupon rack loaded with metal coupons in the ICET tank is illustrated in Figure 3-3. The loading pattern of the racks was nearly identical, varying by only 1 or 2 coupons. Shown in the figure from left to right, the coupons are arranged as follows: 4 Cu, 4 Al, 4 IOZ, 7 GS, 4 Cu, 3 Al, 4 IOZ, 7 GS, 4 Cu, 3 Al, 4 IOZ, 7 GS.

Figure 3-3. Loaded coupon rack in the ICET tank.

Several fiberglass samples were placed in the ICET tank. Samples were either submerged below the water level or held above the water level. The unsubmerged fiberglass samples were positioned so they would be exposed to sprays. The fiberglass samples were contained in stainless steel wire mesh that allowed water flow, while confining the fiberglass material. Both loosely-packed and more tightly-packed samples were used. In addition, some submerged fiberglass samples were located where they would be exposed to relatively high-flow conditions and others were located in regions of the tank with quiescent conditions. Figure 3-4 illustrates the so-called sacrificial fiberglass samples in wire mesh pouches attached to the submerged coupon rack (rack #1 in Figure 3-2). Each pouch contains approximately 5 g of fiberglass. Those samples were attached with SS wire and removed from the tank midway through the test and examined. Bigger insulation bags, those that resemble the two saddle bags in the figure, were wrapped around the sacrificial specimens during the test. See Section 3.3.1 for descriptions of other fiberglass samples.

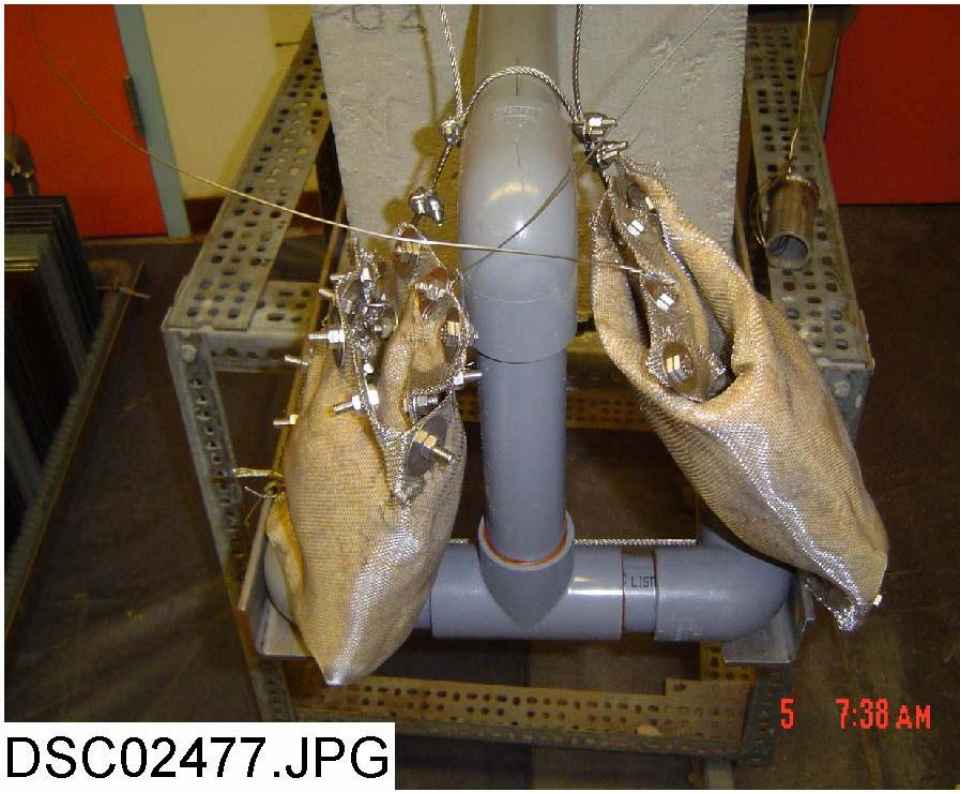

Figure 3-4. Fiberglass samples attached to the submerged coupon rack.

4 EXPERIMENTAL RESULTS

This section begins with a description of the process control settings that were adjusted to match the target conditions specified for Test #2. Then representative results from every type of diagnostic are presented. This information is organized in categories relating more closely to operational activities than to diagnostic methods. Data and photographs are provided here for the (1) coupons, (2) NUKON^{TM} fiberglass samples, (3) concrete samples, (4) time-dependent solution chemistry, (5) precipitated solids, and (6) sediment recovered from the bottom of the tank.

4.1 Test Operation and Sequence

4.1.1. Description

Preparation of ICET Test #2 (Run 2 in Table 3-2) began with the heating of 240 gal. of reverse osmosis (RO) water to 65°C. (Addition of the metal coupons and insulation samples reduces the water temperature by approximately 5°C, so the water was heated initially to 65°C.) With 25 gpm circulating through the loop, the predetermined quantities of boric acid (14.54 kg) and LiOH (0.66 g) were added and dissolved in the ICET tank solution. After the chemicals were added and observed to be well mixed, a baseline grab sample and measurements of the test solution were taken. Then the premeasured latent debris and concrete dust were added to the tank solution. After the solution circulated for 10 minutes, the pump was stopped and the coupon racks and insulation samples were put in the tank.

The test commenced with initiation of the tank sprays, which lasted for 4 hours. Beginning at 30 minutes, Batch 1 of TSP ($Na_3PO_4 \cdot 12H_2O$) solution was metered into the recirculation line. That batch consisted of 300 g of boric acid and 1893 g of TSP in 5 gal. of RO water. When that batch had been injected, after approximately 90 minutes, injection of Batch 2 was begun. Batch 2 consisted of 300 g of boric acid, 1893 g of TSP, and 211 mL of 12.29 N HCl in 5 gal. of RO water. That batch was injected over the remainder of the spray cycle. The sprays were terminated after 4 hours, and the test then continued uninterrupted for the next 30 days. Reference 1 contains details of TSP addition in a PWR.

The experiment commenced at 9:45 A.M. on Saturday, February 5, 2005, and it ended on Monday, March 7, 2005. During the test, grab samples were taken daily for wet chemistry and ICP-AES analyses. Water loss due to water sample removals and evaporation was made up with RO water. Water samples, fiberglass, and metal coupons were analyzed after the test. Sampling and analyses were conducted in accordance with approved project instructions (Refs. 3, 4, and 5).

4.1.2. Process Control

During the test, critical process control parameters were monitored to ensure that the test conditions met the functional test requirements. Recirculation flow rate and temperature

were controlled throughout the test. The solution pH was initially targeted to reach the prescribed value of 7 (Table 3-2) after completion of the spray phase. After that point, pH was not controlled. A summary of the values measured for these parameters during the test follows.

Recirculation flow rate: The average recirculation flow rate was 97.3 L/min (25.7 gpm). Recorded recirculation flow rate had a standard deviation of 0.29 L/min, with a range of 93.4 to 98.8 L/min (24.7 to 26.1 gpm), excluding the spray cycle.

Temperature: Temperature was recorded at three submerged locations in the ICET tank: in two adjacent corners of the tank and directly above the outlet drain. The average recorded temperature at these locations was 60.6°C, 60.4°C, and 60.3°C (141.1°F, 140.7°F, and 140.5°F). The standard deviation in temperature recorded by all three thermocouples was within ±0.27°C (±0.48°F), with a maximum range among all locations of 58.1°C to 61.6°C (136.5°F to 143.0°F).

pH: Prior to test initiation, 14.54 kg of boric acid and 0.66 g of LiOH were dissolved in the ICET tank solution. The measured in-line probe pH was 4.3, which was the expected value obtained from analytical predictions. At test initiation, the in-line probe reading was an unexpectedly high value of 5.61. The bench-top pH meter (which is calibrated before each measurement) provided a similar reading of 5.5, which validated the sudden increase. The addition of latent debris and concrete dust caused the change in pH. TSP Batch 1 and Batch 2 were then metered as described in Subsection 4.1.1. When these prepared batches were added, the in-line probe showed a rise in pH until it reached the value of 7.3, which corresponded to the bench-top reading. After the spray, the in-line pH probe drifted to unreasonably high values that deviated from the bench-top readings. Thus, the bench-top pH values are the only values truly reflective of the solution pH beyond that point. The malfunctioning pH probe was replaced after this test.

Over the first week of Test # 2, the average pH, after the first 4 hours of the test, was 7.2, with a minimum value of pH 7.07 and a maximum value of pH 7.32. During the second week, the average pH rose to 7.3, with a minimum pH of 7.37 and a maximum value of pH 7.42. The average pH remained constant at 7.3 throughout the final 2 weeks of testing. Figure 4-1 shows the pH, as measured by the bench-top pH meter.

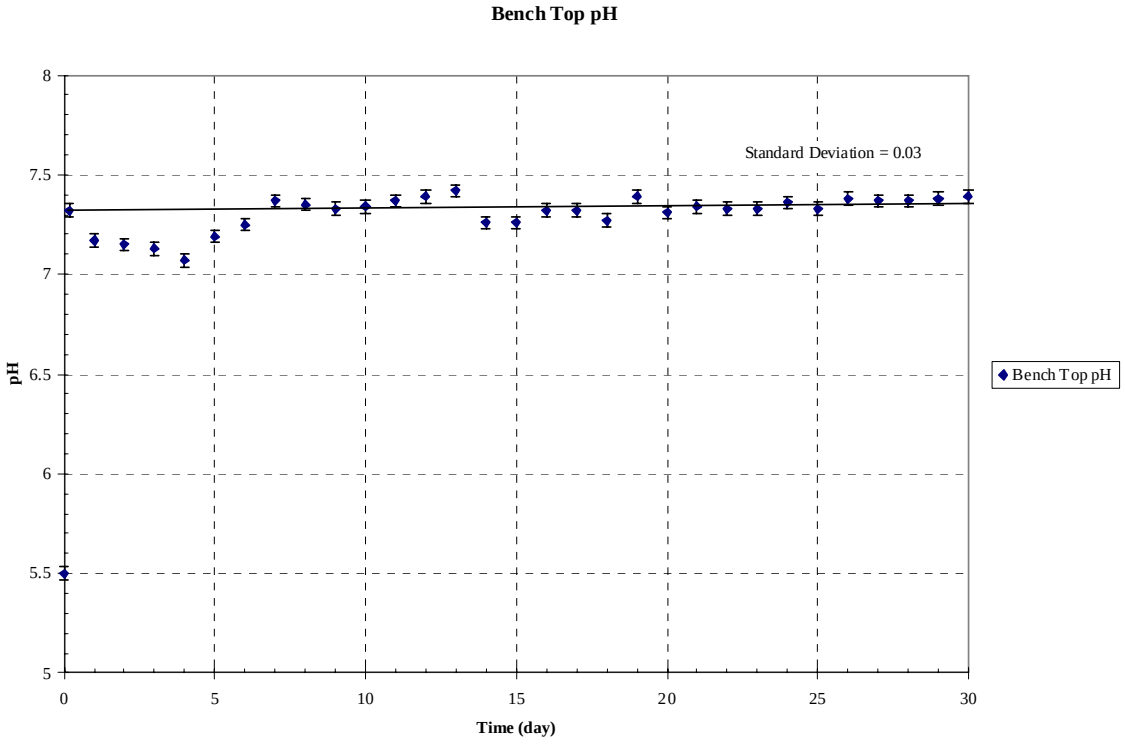

Figure 4-1. Bench-top pH meter results.

4.2 Sample Coupons

4.2.1 Submerged Coupons

Examination of the 40 submerged coupons provides valuable insight into the nature of the chemical kinetics that occurred during this 30-day test. The physical change that these coupons experienced is determined through both visual evidence and weight measurement of each coupon before and after the test. Pre-test pictures were taken of the coupons when they were received and prior to insertion in the racks. Post-test pictures were taken several days after the racks had been removed from the tank. All racks with coupons still inserted were staged to allow complete drying of the coupons prior to the post-test pictures. The coupons were placed in a low-humidity room and allowed to air dry.

During the ICET tests, trace metal cations may be released from the submerged metal coupon surfaces due to corrosion effects. Subsequently, the released metal cations may complex with the anions from the solution through electrostatic interactions, such as OH^-, PO_4^{3-}, SiO_3^{2-}, and CO_3^{2-}. More complicated, the complexated anions may attract other cations from the solution, such as Ca^{2+}, Mg^{2+}, Al^{3+}, Cu^{2+}, Zn^{2+}, and H^+. As a result, corrosion products (deposits) are formed and may continuously grow on the metal coupon surfaces. The thickness of the deposits is in the range of millimeters. On the other hand, corrosion effects may also cause some depressions on the coupon surface. The adherence between the metal coupons and the deposits is through chemical bonds, which

are a much stronger connection than van der Waals forces. Due to the vertical placement of the metal coupons in the tank (with a small horizontal, cross-sectional area), the deposits on the metal coupon surface are likely of chemical origin, rather than being the result of particles settling on the surface.

Figure 4-2 through Figure 4-7 display the pre-test and post-test pictures of the three submerged aluminum coupons. Each post-test aluminum coupon exhibits a similar pattern of white particle deposits. Also, each post-test coupon has a reddish-brown color, which is most attributable to the submerged copper coupons. The relative spatial location of these coupons, given in order from the west side of the tank to the east side of the tank, is as follows: Al-98, Al-97, and Al-96. It is evident that the concentration of white particles increases slightly from the westernmost coupon to the easternmost coupon.

According to SEM/EDS results, the dominant corrosion products on the submerged Al coupons are likely aluminum hydroxide with other substances containing Si, Ca, Na, Mg, P, C, and O. In addition, evidence was found that some Cu deposited on the submerged aluminum coupon surfaces. Comparing the redox potential (E^0) of Al^{3+} and Cu^{2+}, which is –1.662 and 0.3419 V (Ref. 6), respectively, Cu^{2+} in the solution may oxidize Al metal. As a result, Al metal may be oxidized into Al^{3+} and released to the solution. Correspondingly Cu^{2+} is reduced into metallic Cu and subsequently deposits at the aluminum coupon surface.

Figure 4-2. Al-96 submerged, pre-test.

Figure 4-3. Al-96 submerged, post-test.

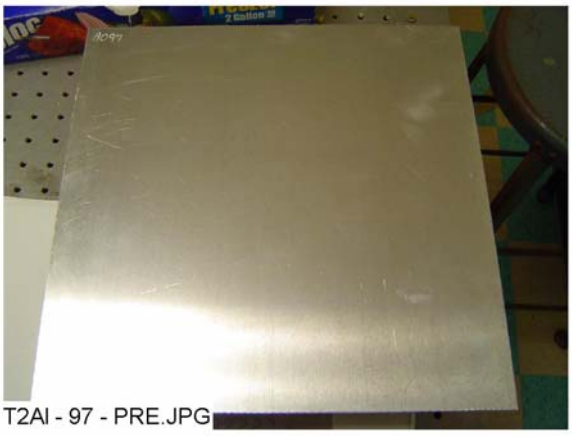

Figure 4-4. Al-97 submerged, pre-test.

Figure 4-5. Al-97 submerged, post-test.

Figure 4-6. Al-98 submerged, pre-test.

Figure 4-7. Al-98 submerged, post-test.

Figure 4-8 through Figure 4-13 present the pre-test and post-test pictures of three submerged galvanized steel coupons. Each post-test galvanized steel coupon exhibits nearly identical patterns of dense gray particle deposits. The relative spatial location of these coupons, given in order from the west side of the tank to the east side of the tank, is as follows: GS-337, GS-338, and GS-335. There is no discernable relationship between the spatial location of the coupons and particle deposition patterns or density. For the submerged galvanized steel coupons, the possible corrosion products are phosphoric and carbonate compounds of Zn and Ca.

Figure 4-8. GS-335 submerged, pre-test.

Figure 4-9. GS-335 submerged, post-test.

Figure 4-10. GS-337 submerged, pre-test.

Figure 4-11. GS-337 submerged, post-test.

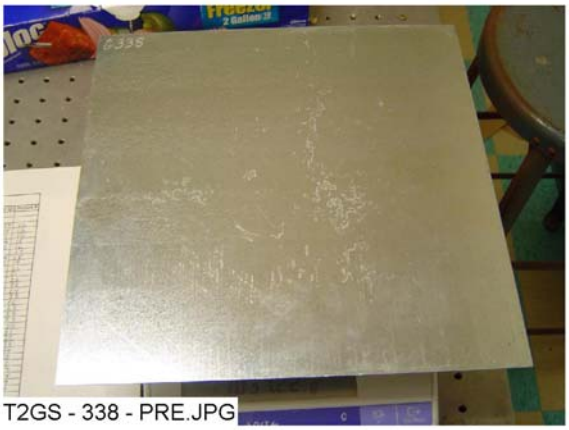

Figure 4-12. GS-338 submerged, pre-test.

Figure 4-13. GS-338 submerged, post-test.

Figure 4-14 through Figure 4-17 present pre-test and post-test pictures of two submerged inorganic zinc-coated steel coupons. Each post-test coated steel coupon exhibits similar

patterns of white particle deposits. The IOZ-81 coupon is located on the west side of the tank in relation to the IOZ-79 coupon. For each coupon, particle deposition appears to preferentially occur near the coupon rack contact points. With respect to the IOZ-81 coupon, the IOZ-79 coupon has more deposits near the top of the coupon and fewer deposits in the bottom corners of the coupon.

Figure 4-14. IOZ-79 submerged, pre-test.

Figure 4-15. IOZ-79 submerged, post-test.

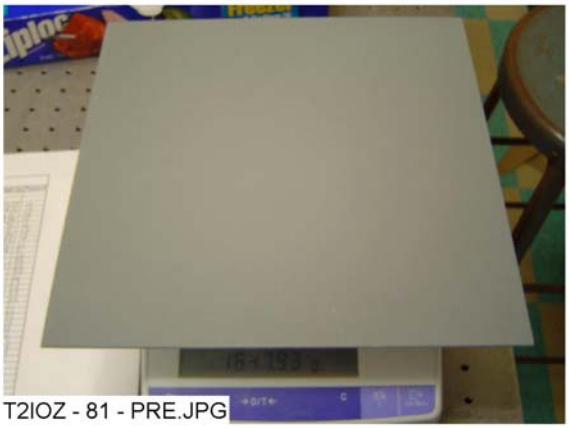

Figure 4-16. IOZ-81 submerged, pre-test.

Figure 4-17. IOZ-81 submerged, post-test.

Figure 4-18 through Figure 4-21 present the pre-test and post-test pictures of two submerged copper coupons. Each post-test copper coupon exhibits similar patterns of white, streak-like deposits. The deposition streaks are almost perfectly horizontal and are more highly concentrated for coupon Cu-123. Different corrosion effects are visible at the contact points. The Cu-123 coupon is located on the west side of the tank in relation to the Cu-105 coupon. The Cu-105 coupon appears to have a greater distribution of these white, streak deposits. For submerged Cu coupons, the possible corrosion products include CuO, $Cu_2(CO_3)(OH)_2$, $Mg_3(PO_4)_2$, and substances containing Mg, Cu, Na, Al, Ca, C, and O.

Figure 4-18. Cu-105 submerged, pre-test.

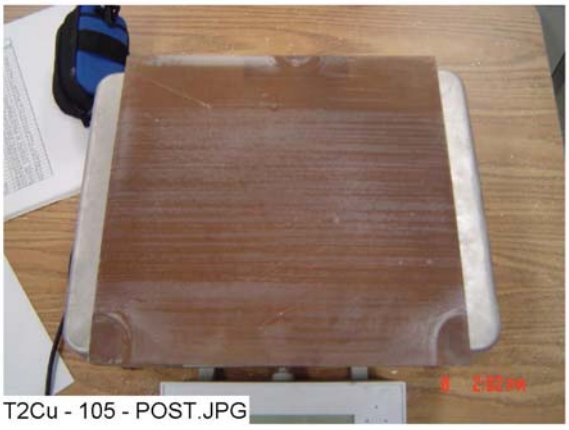

Figure 4-19. Cu-105 submerged, post-test.

Figure 4-20. Cu-123 submerged, pre-test.

Figure 4-21. Cu-123 submerged, post-test.

Figure 4-22 and Figure 4-23 present the pre-test and post-test pictures of the submerged carbon steel coupon. The post-test carbon steel coupon exhibits a reddish-brown color and significant corrosion around the edges. Different corrosion effects are visible at the contact points. This carbon steel coupon was adjacent to a copper coupon. For the submerged steel coupon, the possible corrosion products include phosphoric and carbonate compounds of Fe and Ca and compounds composed by Fe, Al, Si, Na, Ca, Mg, P, and O.

Figure 4-22. US-7 submerged, pre-test.

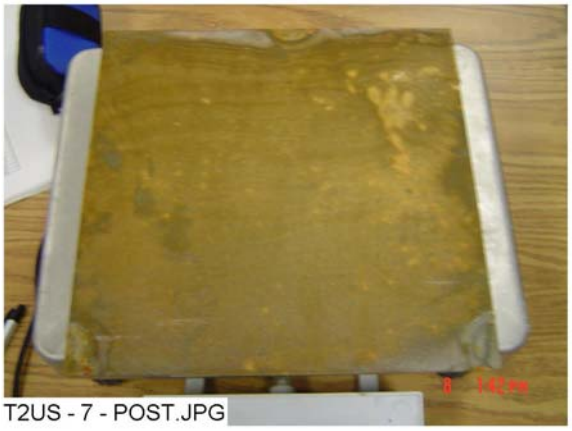

Figure 4-23. US-7 submerged, post-test.

Figure 4-24 and Figure 4-25 present the pre-test and post-test pictures of the submerged concrete coupon. The post-test concrete coupon exhibits an enhanced gray color as compared with the pre-test coupon.

Figure 4-24. Conc-002 submerged, pre-test.

Figure 4-25. Conc-02 submerged, post-test.

Table 4-1 presents the pre-test and post-test weight data for each representative submerged coupon shown in Figures 4-2 through 4-25, while the average weight changes for each test material is summarized in Table 4-2.

Table 4-1. Weight Data for Submerged Coupons

Type	Coupon No.	Pre-Test Wt. (g)	Post-Test Wt. (g)	Net Gain/Loss (g)
Al	96	393.1	391.7	-1.4
Al	97	392.3	391.8	-0.5
Al	98	391.9	391.1	-0.8
GS	335	1055.8	1084.6	28.8
GS	337	1052.7	1086.1	33.4
GS	338	1057.2	1084.5	27.3
IOZ	79	1654.5	1658.8	4.3
IOZ	81	1647.9	1651.6	3.7
Cu	105	1316.5	1316.6	0.1
Cu	123	1314.5	1314.5	0.0
US	7	1025.1	1026.5	1.4
Conc	2	7191.0	7431.7	240.7

The aluminum coupons lost an average of 0.9 g, which represents 0.23% of the pre-test coupon weight. The galvanized steel coupons gained an average of 29.8 g, which is 2.83% of the original coupon weight. The coated steel coupons' mean weight gain was 4.0 g, which is 0.24% of the pre-test coupon weight. The copper coupons, on average, did not experience any discernable weight gain. The carbon steel coupon gained 1.4 g, which represents 0.14% of its original weight. Finally, the concrete coupon gained 240.7 g, which is 3.35% of its pre-test weight. The concrete weight gain is likely due to retained water absorption.

Table 4-2. Weight Gains for Submerged Coupons

Submerged Coupons		
Coupon Type	**Weight (g) Gain/Loss (–)**	**Weight Gain/Loss (–) (% of Pre-Test Weight)**
Al	–0.9	–0.2
GS	28.6	2.7
Cu	<0.1	<0.1
IOZ	3.8	0.2
US	1.4	0.1
Concrete	240.7	3.4

4.2.2 Unsubmerged Coupons

The physical and chemical changes that the unsubmerged coupons experienced during Test #2 are less significant than the submerged coupons. Figure 4-26 through Figure 4-29 demonstrate the pre-test and post-test pictures of two unsubmerged aluminum coupons. Each post-test aluminum coupon exhibits similar deposits. Also, the texture of each coupon is coarser and the surface is less lustrous than its pre-test appearance. The reddish-brown color that was observed on the submerged coupons is absent on the unsubmerged coupons. The Al-101 coupon was loaded into rack 2, which was located in the southern position on the tank's middle tier (see Figure 3-2). The Al-132 coupon was loaded into rack 5, which was located in the southern position of the tank's top tier. The Al-101 specimen exhibits a greater concentration of these deposits.

Figure 4-26. Al-101 unsubmerged, pre-test.

Figure 4-27. Al-101 unsubmerged, post-test.

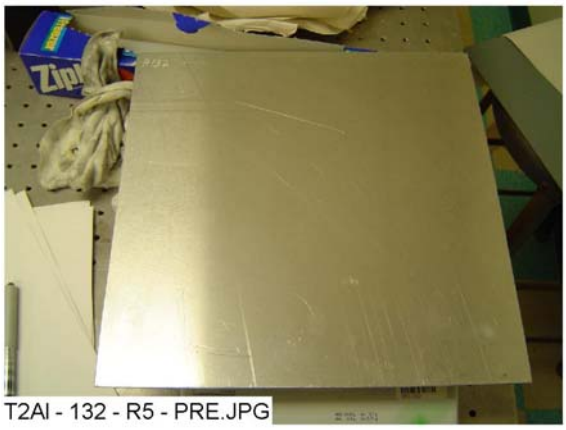

Figure 4-28. Al-132 unsubmerged, pre-test.

Figure 4-29. Al-132 unsubmerged, post-test.

Figure 4-30 through Figure 4-33 show the pre-test and post-test pictures of two unsubmerged galvanized steel coupons. Each post-test galvanized steel coupon exhibits

similar types of deposits. This deposition is visibly different and much less concentrated than that of the submerged coupons. The GS-366 coupon was loaded in rack 3, which was located in the center position of the tank's middle tier. The GS-416 coupon was loaded in rack 5, which was located in the southern position of the tank's top tier. The GS-366 coupon exhibits more of these deposits.

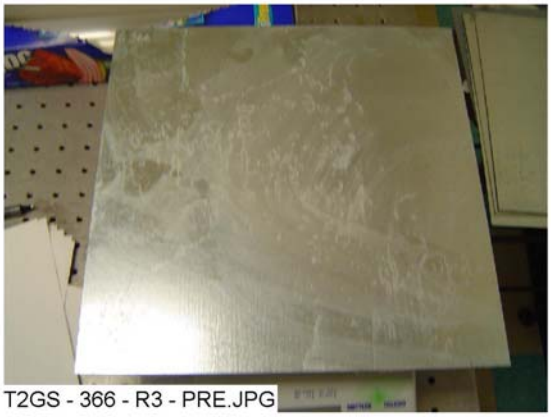

Figure 4-30. GS-366 unsubmerged, pre-test.

Figure 4-31. GS-366 unsubmerged, post-test.

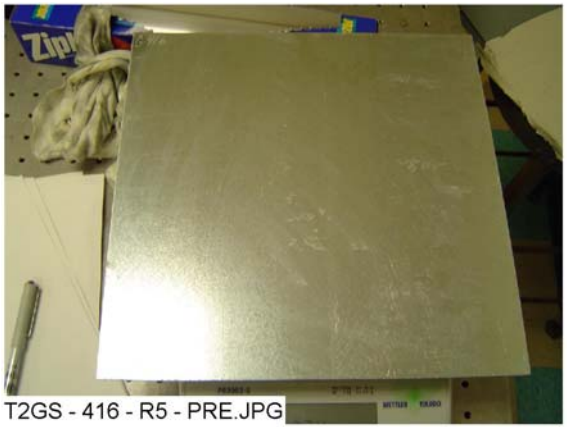

Figure 4-32. GS-416 unsubmerged, pre-test.

Figure 4-33. GS-416 unsubmerged, post-test.

Figure 4-34 through Figure 4-37 present the pre-test and post-test pictures of two unsubmerged copper coupons. Each post-test copper coupon exhibits similar types of deposits. Unlike on the submerged coupons, the deposition patterns are vertical and less uniform. The Cu-154 coupon was loaded in rack 4, which was located in the northern position of the tank's middle tier. The Cu-196 coupon was loaded in rack 7, which was located in the northern position of the tank's top tier. The Cu-196 coupon exhibits a greater density of these white deposits.

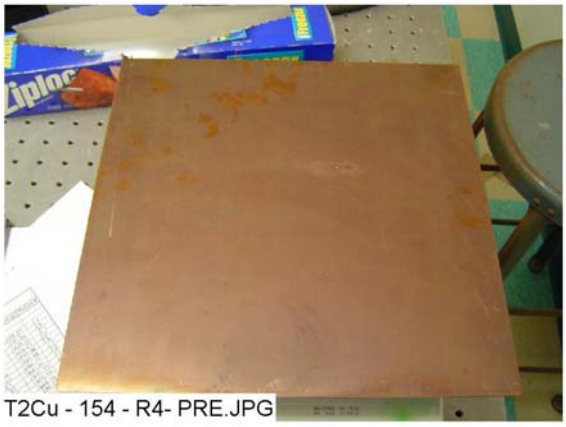

Figure 4-34. Cu-154 unsubmerged, pre-test.

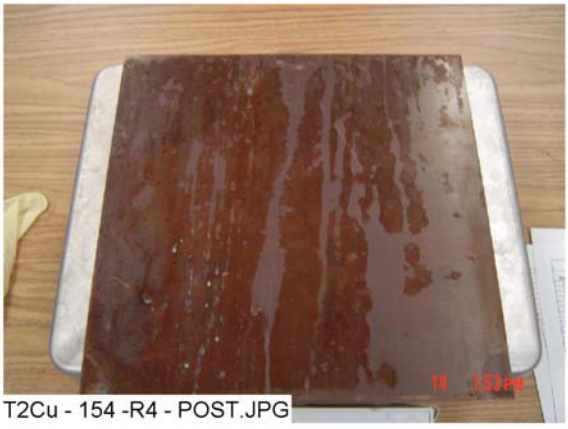

Figure 4-35. Cu-154 unsubmerged, post-test.

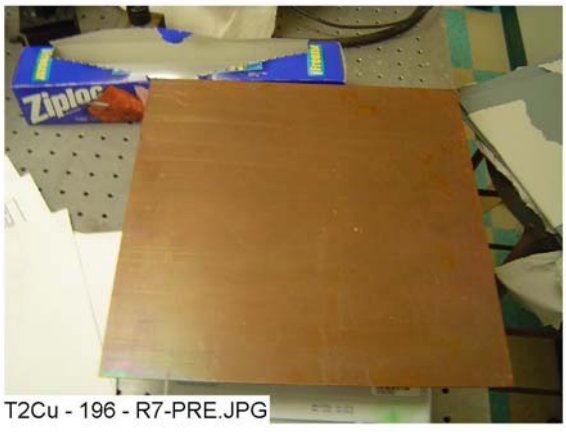

Figure 4-36. Cu-196 unsubmerged, pre-test.

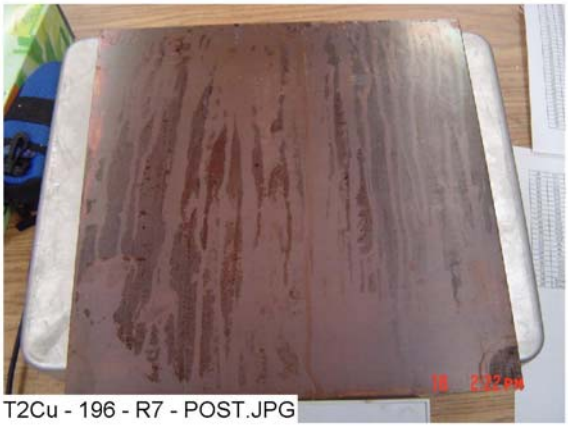

Figure 4-37. Cu-196 unsubmerged, post-test.

Figure 4-38 through Figure 4-41 present the pre-test and post-test pictures of two unsubmerged inorganic zinc coated steel coupons. Each post-test coated steel coupon exhibits similar types of deposits. These deposits are much less concentrated than the deposits on the submerged coupons. The IOZ-86 coupon was loaded in rack 2, which was located in the southern position of the tank's middle tier. The IOZ-135 coupon was loaded in rack 6, which was located in the center position of the tank's top tier. There are no apparent differences in the IOZ coupons as a function of coupon location.

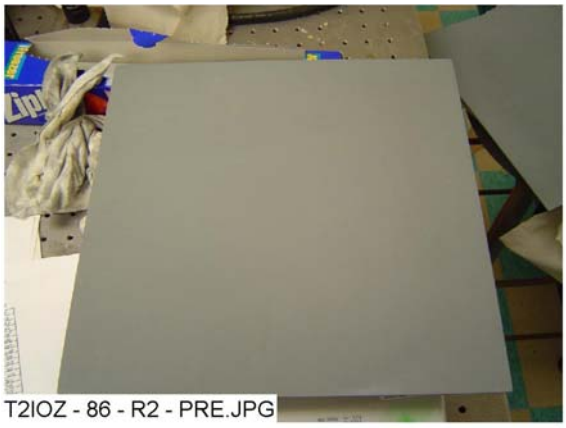

Figure 4-38. IOZ-86 unsubmerged, pre-test.

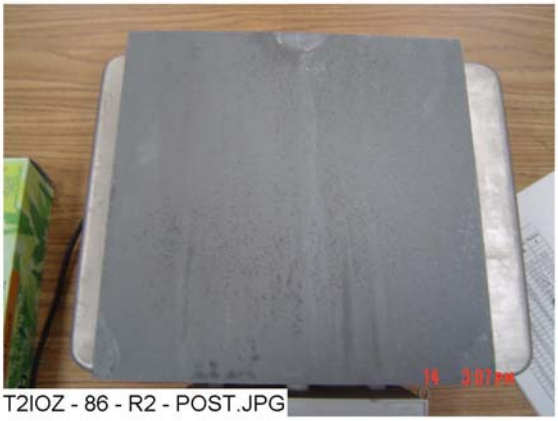

Figure 4-39. IOZ-86 unsubmerged, post-test.

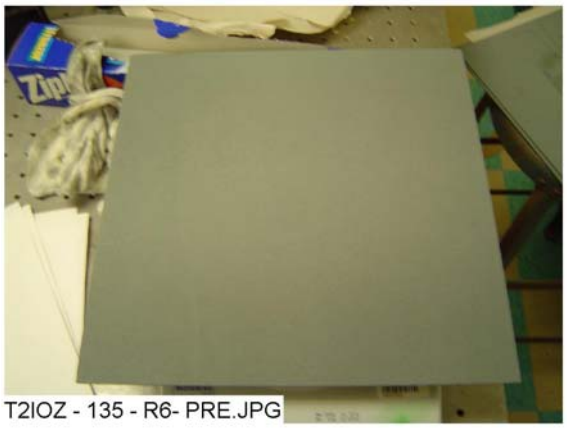

Figure 4-40. IOZ-135 unsubmerged, pre-test.

Figure 4-41. IOZ-135 unsubmerged, post-test.

Figure 4-42 and Figure 4-43 present the pre-test and post-test pictures of one unsubmerged carbon steel coupon. The post-test carbon steel coupon exhibits a reddish-

brown color and significant corrosion around the edges. The color is similar to that of the submerged carbon steel coupon, although the corrosion does not appear to be as severe as on the submerged coupon. The US-10 coupon was loaded in rack 6, which was in the center position of the tank's top tier.

Figure 4-42. US-10 unsubmerged, pre-test.

Figure 4-43. US-10 unsubmerged, post-test.

Table 4-3 presents the pre-test and post-test weight data for each representative unsubmerged coupon shown in Figures 4-26 through 4-43. Shown in Table 4-4 are the average weight gains by coupon type for each unsubmerged rack. Table 4-5 provides the average percentage weight gain for each unsubmerged rack.

Table 4-3. Weight Data for Unsubmerged Coupons

Type	Coupon No.	Pre-Test Wt. (g)	Post-Test Wt. (g)	Net Gain/Loss (g)
Al	101	392.3	392.5	0.2
Al	132	391.3	392.3	1.0
GS	366	1061.8	1062.0	0.2
GS	416	1060.3	1061.1	0.8
IOZ	86	1599.1	1600.6	1.5
IOZ	135	1606.2	1608.2	2.0
Cu	154	1310.4	1310.6	0.2
Cu	196	1296.7	1296.7	0.0
US	10	1028.4	1029.3	0.9

Overall the unsubmerged coupons experienced fairly uniform weight gains. The aluminum coupons gained an average of 0.4 g, which represents 0.1% of the pre-test coupon weight. The galvanized steel coupons gained an average of 0.4 g, which is 0.04% of the original coupon weight. The coated steel coupons' mean weight gain was 1.7 g, which is 0.1% of the pre-test coupon weight. The copper coupons' mean weight gain was less than 0.1 g, which was less than 0.01% of the pre-test weight. The carbon steel coupons gained an average of 1.3 g, which represents 0.13% of its original weight. Each of the net percentage weight gains is below 0.2%.

Generally, the unsubmerged coupons experienced less weight change than the submerged coupons (Table 4-2). Specifically, the weight gain for the unsubmerged galvanized steel coupons is significantly less than for the submerged coupons. The unsubmerged zinc coated steel weight gain was approximately half of the submerged coupon gain. The weight gain of the unsubmerged aluminum specimens contrast the weight loss in the submerged aluminum specimens. Some differences in weight gain between racks is seen in Table 4-4, however, they are minor. Observations of the post-test coupons in their racks did not reveal a pattern of corrosion other than random differences between coupons.

Table 4-4. Weight Gains for Unsubmerged Coupons

Unsubmerged Coupons					
	Mean Weight (g) Gain or Loss (-) by Coupon Type				
Rack No.	Al	GS	Cu	IOZ	US
2	0.6	0.2	<0.1	1.7	NA
3	<0.1	0.2	<0.1	0.7	NA
4	0.2	0.3	<0.1	1.5	1.7
5	1.0	0.7	-0.1	2.5	NA
6	0.3	0.6	<0.1	2.2	0.9
7	0.5	0.5	<0.1	1.6	NA
Overall	0.4	0.4	<0.1	1.7	1.3

Table 4-5. Coupon Weight Gain as a Percent of Pre-Test Weight

Unsubmerged Coupons					
	Weight Gain or Loss (-) by Coupon Type (% of Pre-Test Weight)				
Rack No.	**Al**	**GS**	**Cu**	**IOZ**	**US**
2	0.16	0.02	<0.01	0.11	NA
3	<0.01	0.02	<0.01	0.04	NA
4	0.05	0.02	<0.01	0.09	0.17
5	0.25	0.06	-0.01	0.15	NA
6	0.07	0.05	<0.01	0.13	009
7	0.11	0.05	<0.01	0.1	NA
Overall	0.1	0.04	<0.01	0.1	0.13

4.3 NUKON™ Fiberglass Samples

4.3.1 Fiberglass Sample Description

The NUKON™ fiberglass provided for the ICET tests was heat treated on one side at 600ºF for 24 hours and run through a leaf shredder twice. For Test #2, 4.58 ft^3 of NUKON™ fiberglass enclosed in a fine SS mesh was placed in the tank. Of this amount, 75% was submerged below the water level, and 25% was placed above the water level and exposed to sprays. For more information on the chemical content of the fiberglass, see Reference 2.

4.3.2 Deposits in Fiberglass

The fiberglass debris was contained in SS mesh bags to minimize migration of the fiberglass throughout the tank and piping. Small mesh envelopes approximately 4-in. square, containing approximately 5 g of fiber, were pulled out of the tank periodically for SEM examination. These sample envelopes were placed in a range of water flow conditions, but none experienced direct water flow through the fiber. All were thoroughly immersed in the test solution until they were recovered from the tank.

There were four locations of fiberglass in the tank that were examined in this test, including the low-flow area, the high-flow area, the birdcage, and the drain collar. (See Section 3.3.1 for descriptions of fiberglass samples.) Both the exterior and the interior of the fiberglass samples from each location were examined. In Subsections 4.3.2.1 through 4.3.2.6, the ESEM/SEM/EDS results are presented according to the location of the fiberglass samples in the tank and the sampling date. The different samples include unused, clean fiberglass; Day 16 low flow; Day 30 low flow; Day 30 high flow; Day 30 birdcage; and Day 30 drain collar. The corresponding figures are Figures 4-44 through 4-69.

Figure 4-44 illustrates the appearance of clean fiberglass before exposure to the chemical environment. After the fiberglass was exposed to the tank solution for some time, deposits formed throughout the fiber matrix and appear to be chemically originated and/or physically retained or attached. Because there was no direct water flow through the fiber, particle migration into the fiberglass interior is likely not the source of these deposits. Therefore, the deposits found in the interior of the fiberglass samples are likely chemically originated, i.e., through precipitation. However, particulate deposits may be physically retained or attached on the fiberglass exterior. Thus, the particulate deposits are more likely on the exterior of the fiberglass samples than on the interior.

In general, the deposits appear to be more prevalent and/or to develop as the test proceeds. The figures show that the deposits are pervasive throughout the fiber. However, the particulate deposits are more significant in the exterior fiberglass samples, while flocculence was more prevalent in the interior fiberglass samples. Comparing the probe SEM results to ESEM results, much more significant flocculence was found with probe SEM analysis, especially for the interior fiberglass samples. The possible reason is that ESEM samples were moist compared to the dry, probe SEM samples during the examination process, and the drying process caused the formation of the flocculent deposits, i.e., chemical precipitation. In addition, the EDS results indicate a large number of elemental constituents in these deposits, including O, Na, Mg, Al, P, Ca, and possibly Si. These elements likely originated from the metal and concrete coupons, fiberglass, and testing solution. Comparing the amount of debris attached on fiberglass at different locations revealed more debris on the drain collar and birdcage fiberglass samples than on the high- and low-flow samples. No significant difference in the amount of deposits was observed between high- and low-flow samples.

4.3.2.1 Clean Fiberglass

Figure 4-44 illustrates the clean fiberglass as it appears prior to the test. This visual baseline is used to compare with images from samples taken after the test began. As can be seen, there are no deposits on the clean fiberglass.

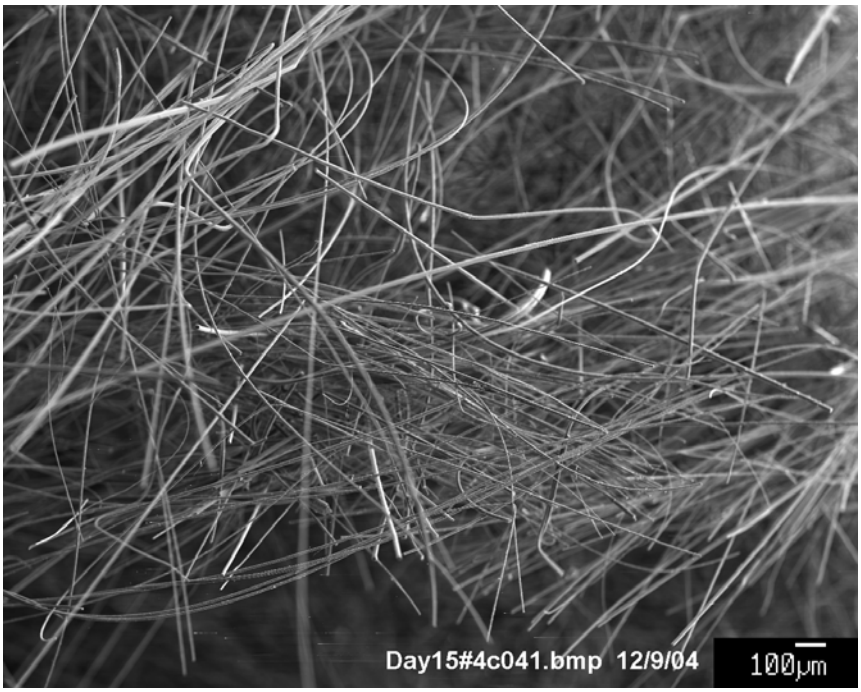

Figure 4-44. Clean fiberglass before exposure to test chemicals.

4.3.2.2 Day 16 Low-Flow Fiberglass Samples

Based on the SEM results, deposits were found after 16 days of the test on both the interior and the exterior of the low-flow fiberglass samples. There was no significant difference in the amounts of deposits on the interior and exterior samples.

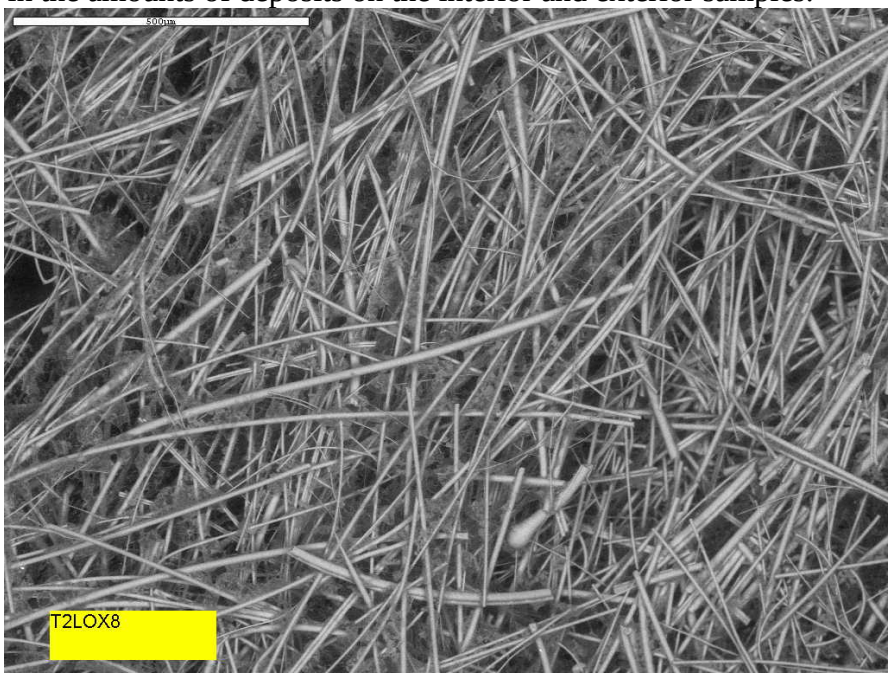

Figure 4-45. ESEM image overview for the Test #2 Day 16 exterior low-flow fiberglass sample.

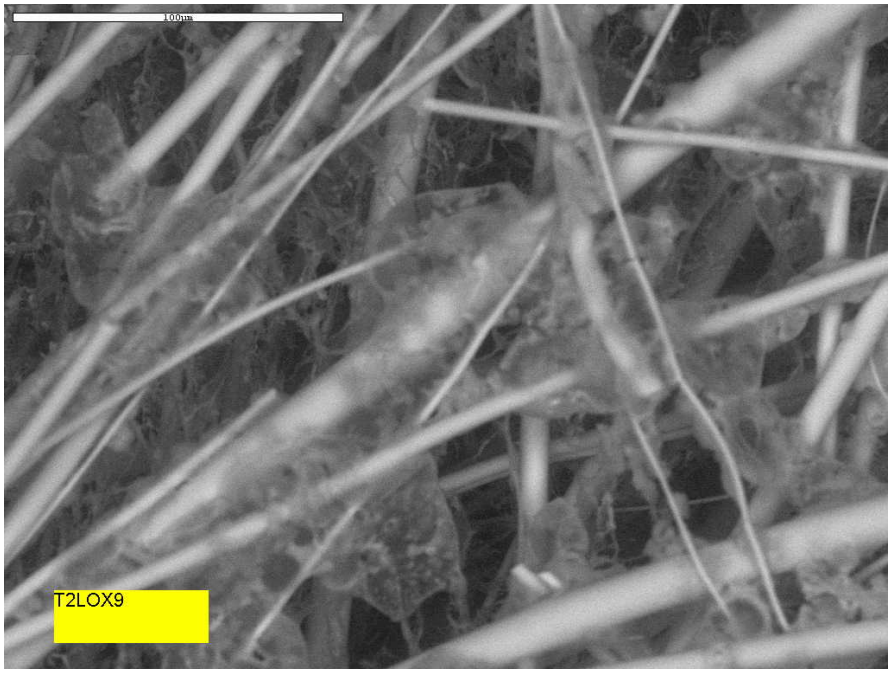

Figure 4-46. Higher-magnification ESEM image of a Test #2 Day 16 exterior low-flow fiberglass sample.

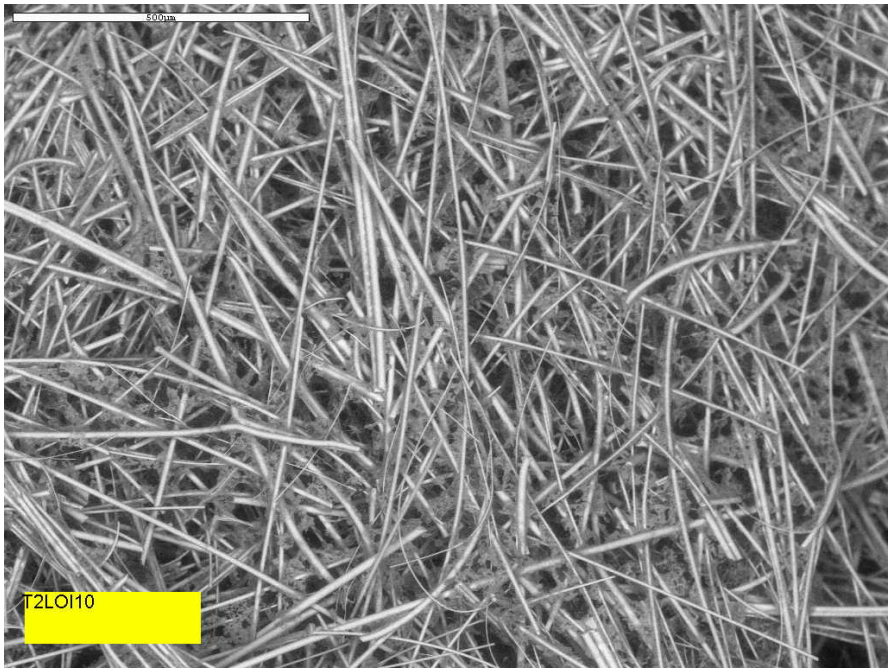

Figure 4-47. ESEM image overview of a Test #2 Day 16 interior low-flow fiberglass sample.

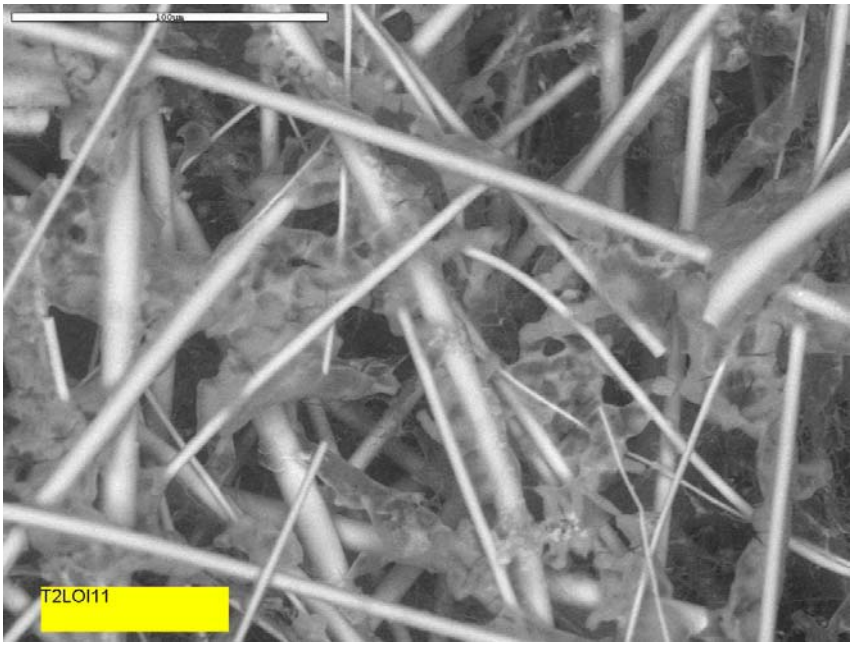

Figure 4-48. Higher-magnification ESEM image of a Test #2 Day 16 interior low-flow fiberglass sample.

4.3.2.3 Day 30 Low-Flow Fiberglass Samples

On Day 30, more particulate deposits were found on the exterior of low-flow fiberglass samples than were found on Day 16. As the test proceeded from Day 16 to Day 30, particulate deposits had a greater chance of being retained or attached to fiberglass. Comparing the two samples revealed slightly more deposits on the Day 30 interior low-flow fiberglass sample than on the Day 16 sample. Comparing the exterior and the interior of Day 30 low-flow fiberglass samples revealed more particulate deposits on the exterior sample.

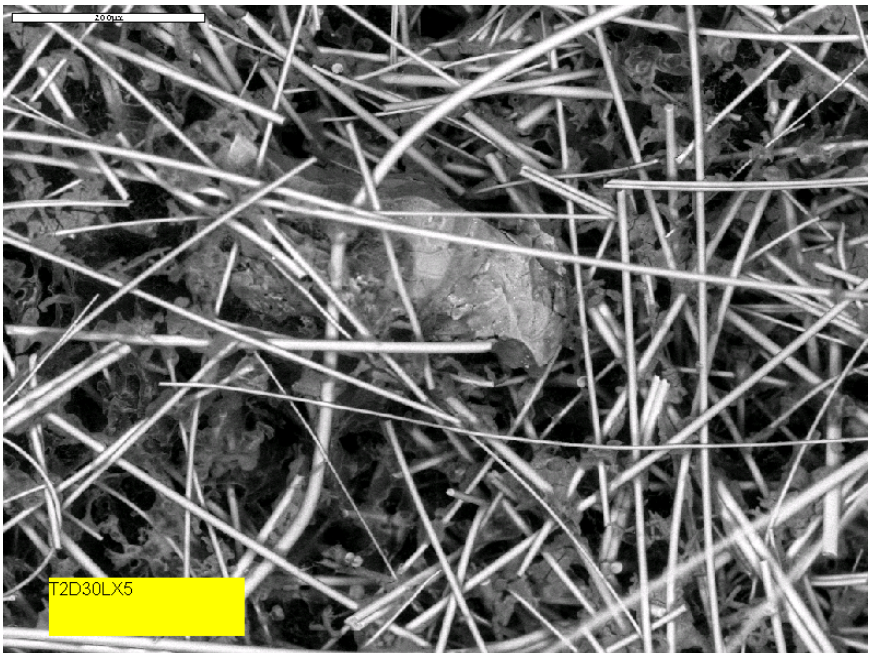

Figure 4-49. ESEM image for a Test #2 Day 30 low-flow exterior fiberglass sample.

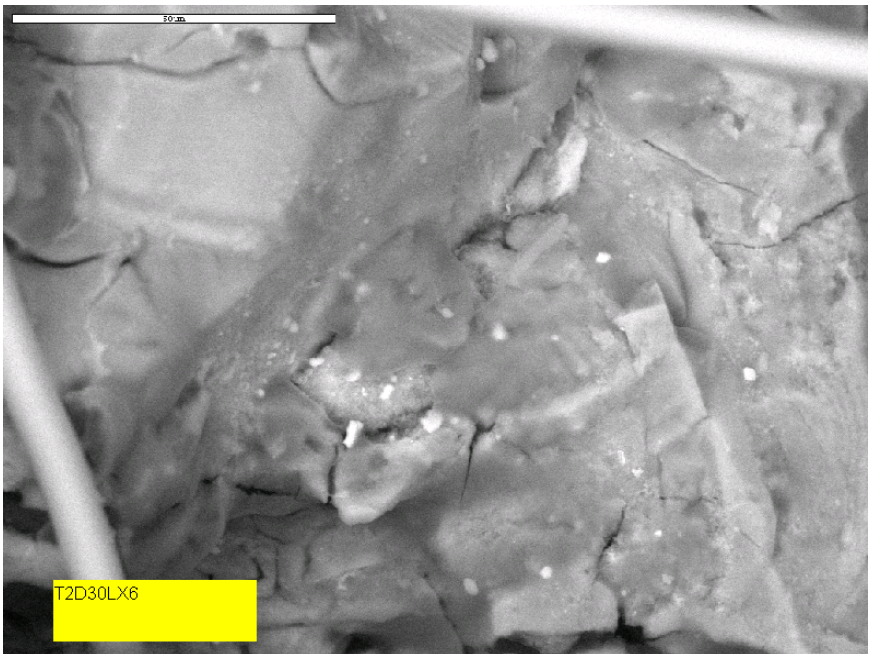

Figure 4-50. Higher-magnification ESEM image of a Test #2 Day 30 low-flow exterior fiberglass sample.

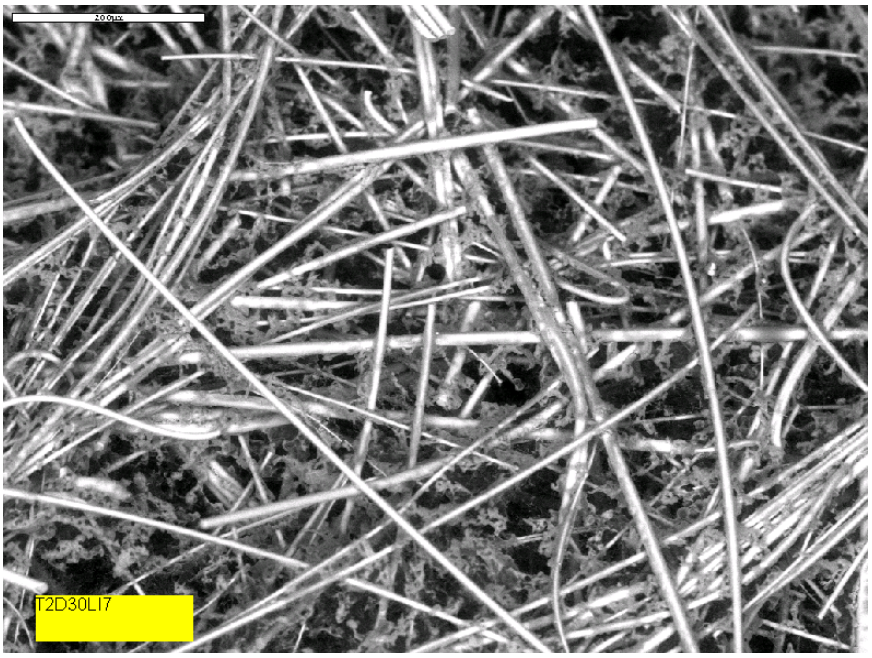

Figure 4-51. ESEM image of a Test #2 Day 30 low-flow interior fiberglass sample.

Figure 4-52. Higher-magnification ESEM image of a Test #2 Day 30 low-flow interior fiberglass sample.

4.3.2.4 Day 30 High-Flow Fiberglass Samples

In the Day 30 high-flow fiberglass samples, significantly fewer particulate deposits were found on the interior samples than on the exterior samples. However, there is no apparent difference between Day 30 high- and low-flow fiberglass samples. The possible reason is that the total suspended solid (TSS) concentration was generally low in Test #2 (~10 mg/L).

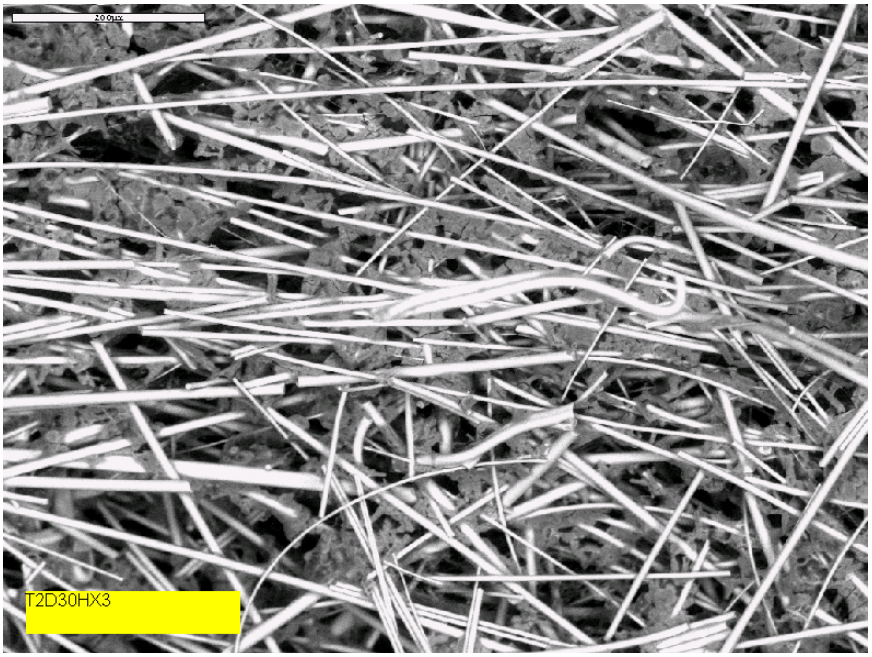

Figure 4-53. ESEM image for a Test #2 Day 30 high-flow exterior fiberglass sample.

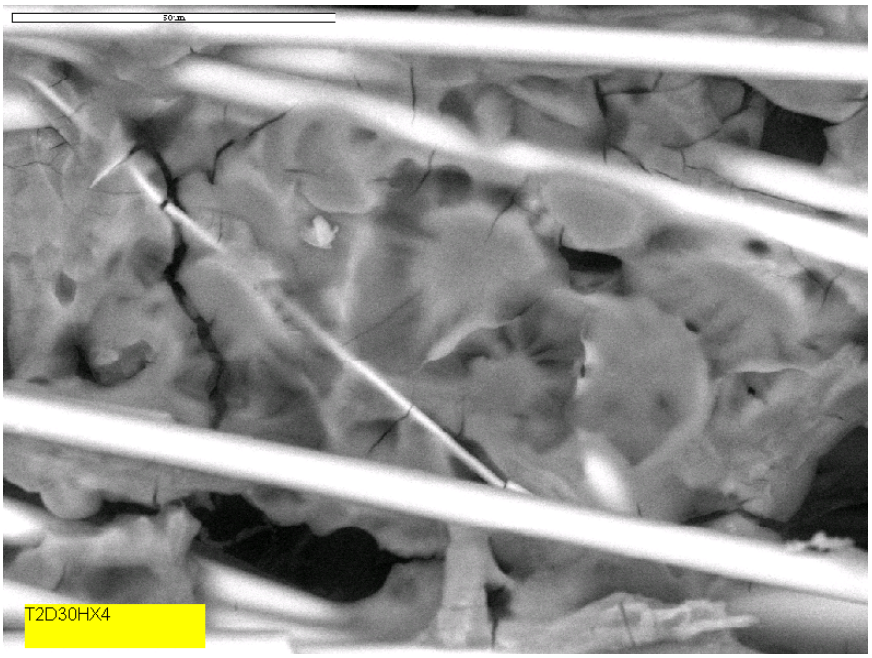

Figure 4-54. Higher-magnification ESEM image of a Test #2 Day 30 high-flow exterior fiberglass sample.

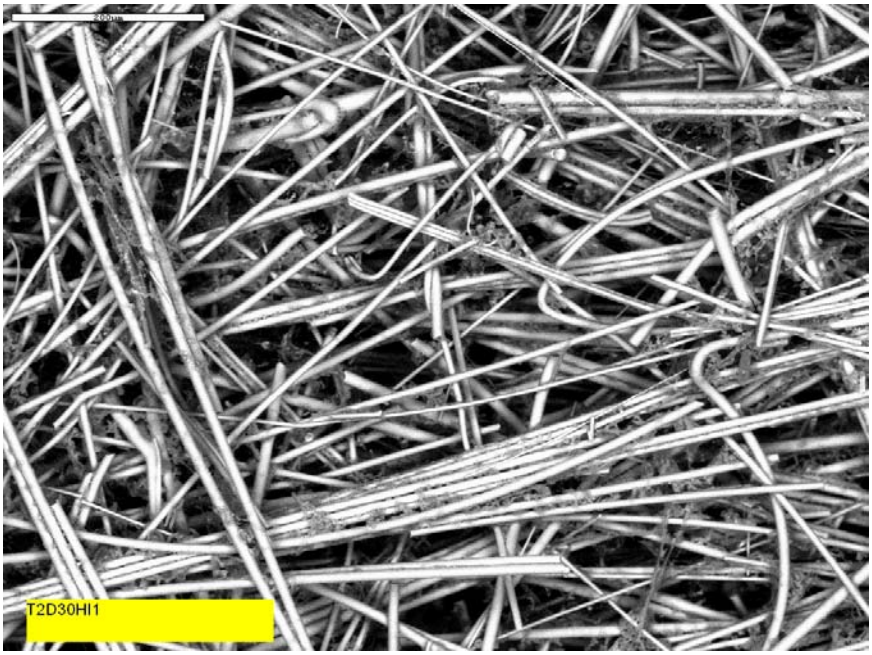

Figure 4-55. ESEM image for a Test #2 Day 30 high-flow interior fiberglass sample. It seems that the interior fiberglass is cleaner than exterior samples.

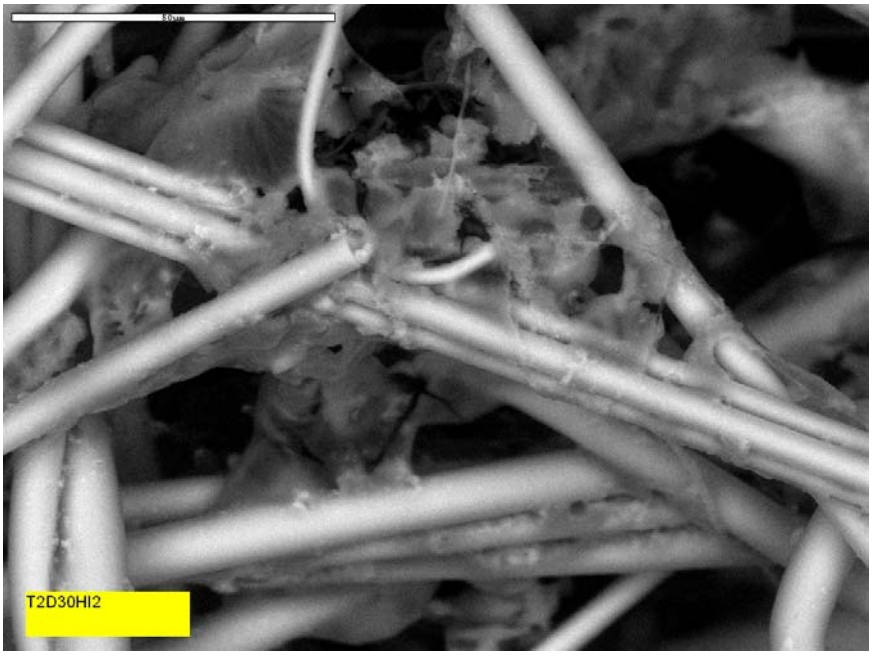

Figure 4-56. Higher-magnification ESEM image of a Test #2 Day 30 high-flow interior fiberglass sample.

4.3.2.5 Day 30 Fiberglass Sample within the Birdcage

For the Day 30 fiberglass sample within the birdcage, Figure 4-57 indicates a coating over the exterior of the fiberglass. It shows the development of a continuous coating, which includes particles that were likely physically deposited or attached. In addition, Figure 4-58 shows the presence of lathlike crystals in the exterior of the fiberglass sample. The crystals may have been physically deposited or originated from chemical precipitation. The EDS result (Figure 4-59) shows that the crystal is composed of C, O, Na, Ma, P, and Ca.

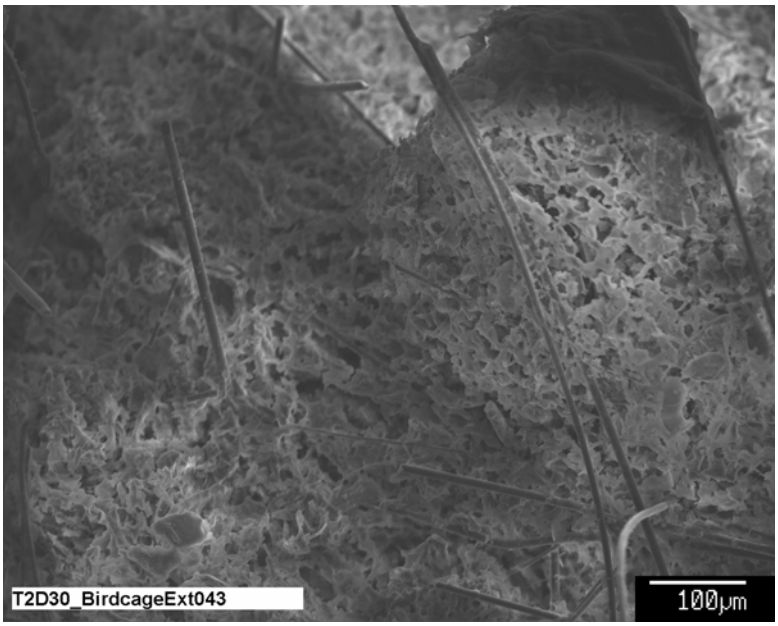

Figure 4-57. SEM image of a Test #2 Day 30 exterior fiberglass sample within the birdcage.

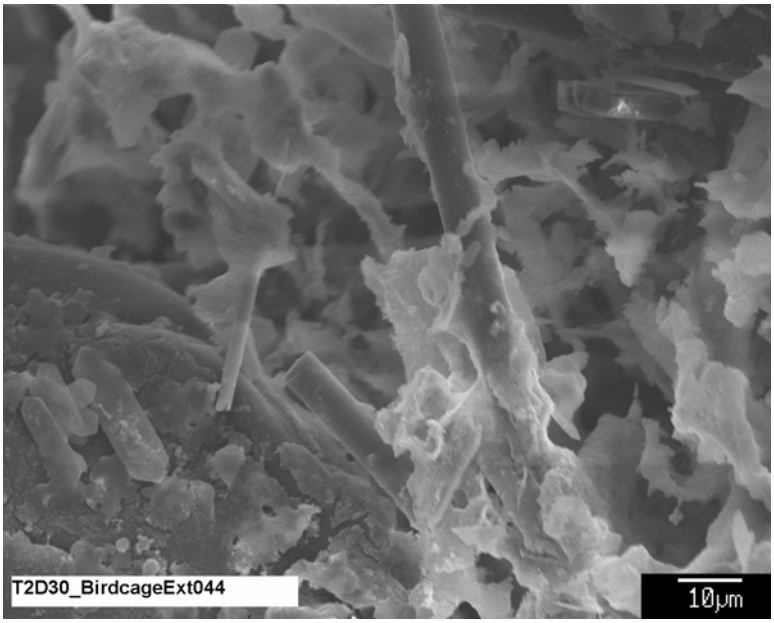

Figure 4-58. Higher-magnification SEM image of a Day 30 exterior fiberglass sample within the birdcage.

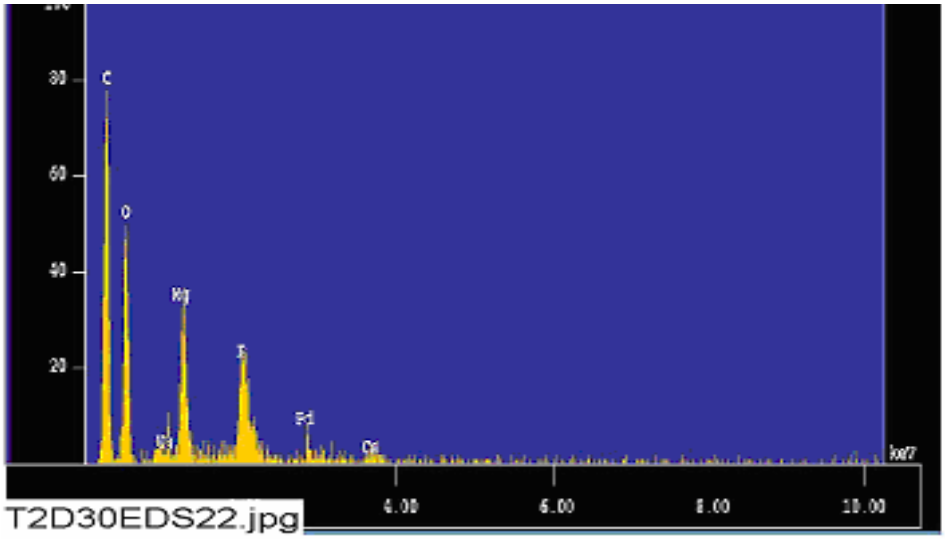

Figure 4-59. EDS counting spectrum for the lathlike crystal on the lower left side of Figure 4-58. From left to right, the element peaks are C, O, Na, Mg, P, Pd (coating substance for SEM analyses), and Ca.

Different from the exterior, the birdcage interior fiberglass sample had no significant particulate deposits or crystal material attached (see Figures 4-60 and 4-61). Instead, flocculent deposits were dominant. Because there was no direct water flow through the fiber, the migration of particles into the fiberglass interior is less likely. Therefore, the flocculent deposits found in the interior samples were likely formed by chemical precipitation. EDS results (Figure 4-62) indicate that the flocculence is composed of O, Na, Mg, Si, Al, P, and Ca.

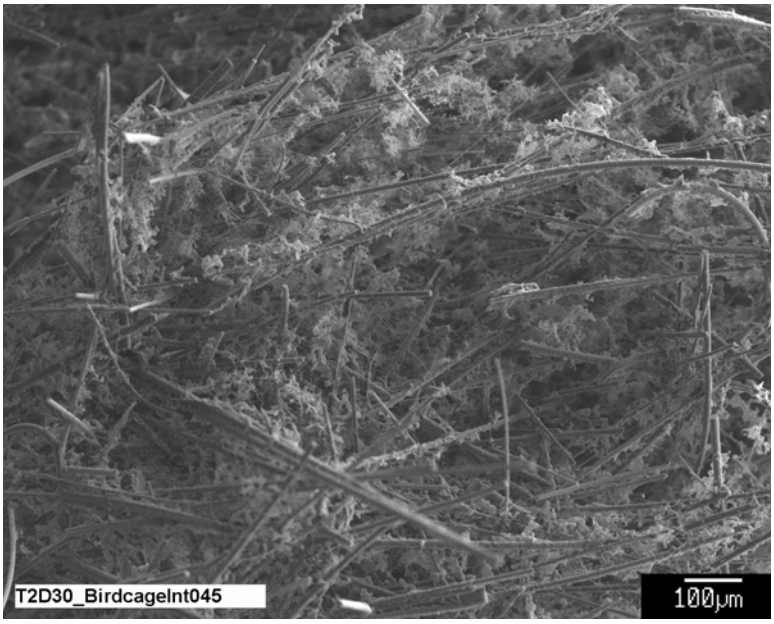

Figure 4-60. SEM image of a Test #2 Day 30 interior fiberglass sample within the birdcage.

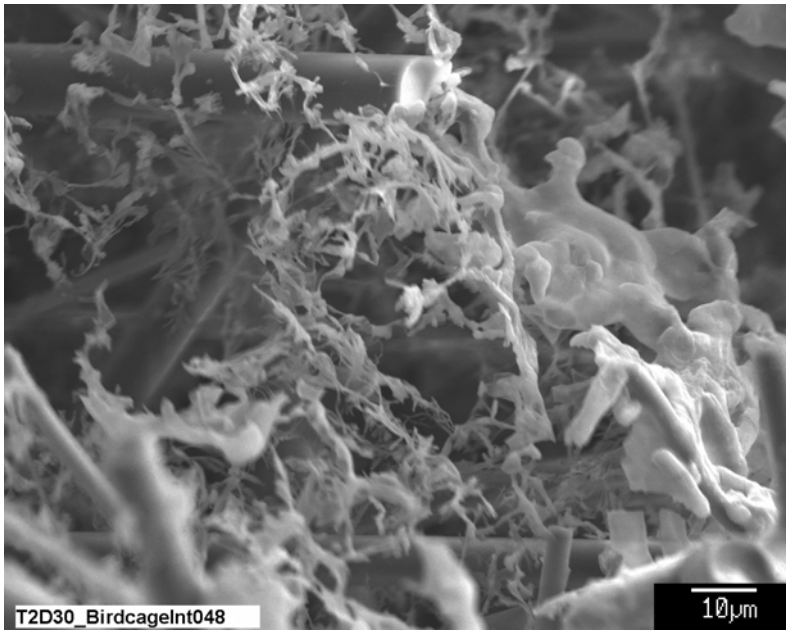

Figure 4-61. Higher-magnification SEM image of a Test #2 Day 30 interior fiberglass sample within the birdcage.

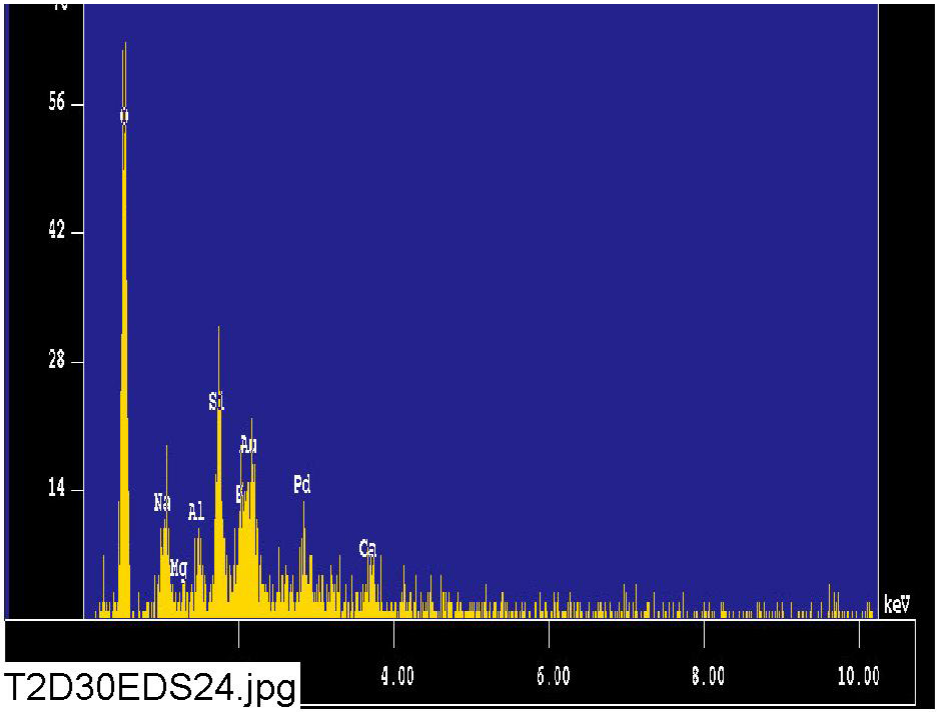

Figure 4-62. EDS counting spectrum for the flocculence on the fiberglass, as shown in Figure 4-61. From left to right, the element peaks are O, Na, Mg, Al, Si, P, Au, Pd, and Ca. (Au and Pd are coating substances for SEM analyses.)

4.3.2.6 Day 30 Drain Collar Fiberglass Samples

More particulate deposits were observed on the exterior of the Day 30 drain collar fiberglass sample than on the interior. The amount of the deposits on the sample farthest from the drain screen was greater than the amount on the sample next to the drain screen, which was greater than the amount in the drain collar interior. Consistent with the birdcage fiberglass samples, the flocculent deposits was dominant in the interior drain collar samples. EDS results show that the particulate deposits on the drain collar exterior were composed of C, O, Na, Mg, Al, Si, P, and Ca. Figures 4-63 through 4-69 illustrate these findings.

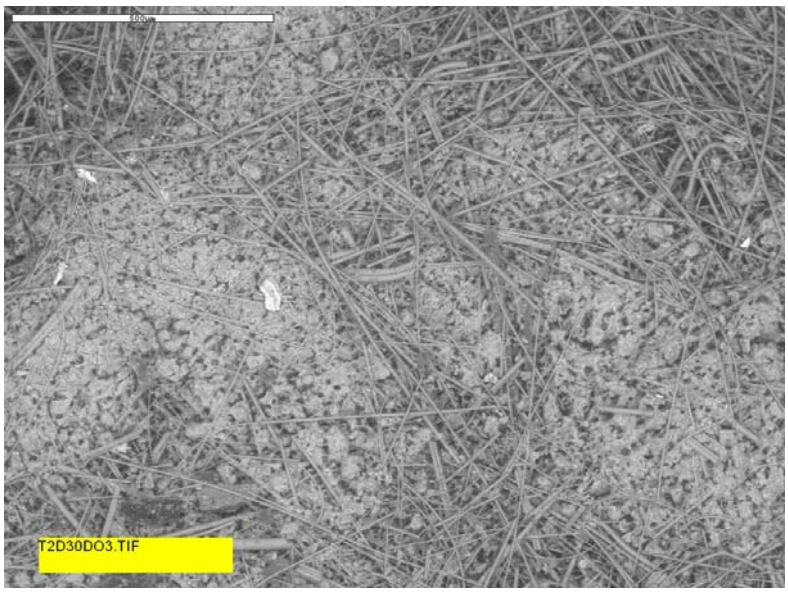

Figure 4-63 ESEM image of a Test #2 Day 30 exterior fiberglass sample on the drain collar (away from the drain screen). The image shows a great amount of particulate deposits on the fiberglass.

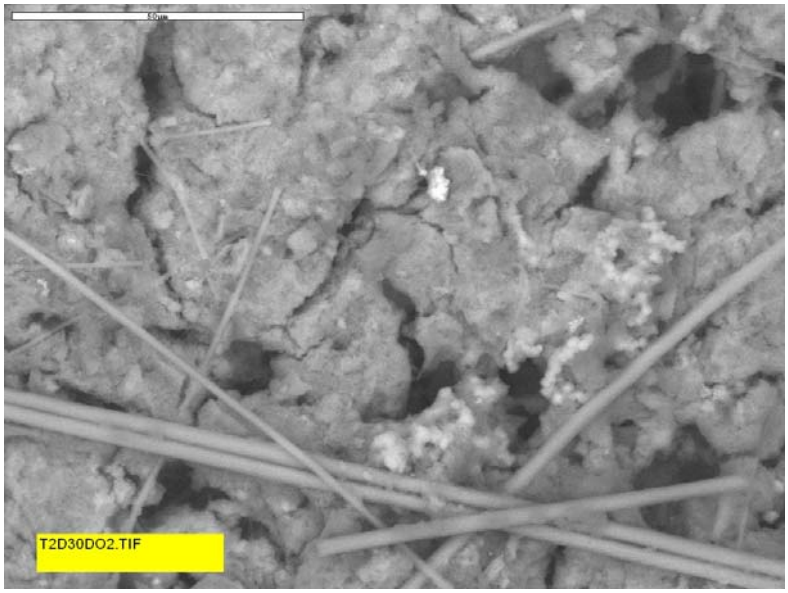

Figure 4-64. Higher-magnification ESEM image of a Test #2 Day 30 exterior fiberglass sample on the drain collar (away from the drain screen). The image shows particulate deposits on the fiberglass.

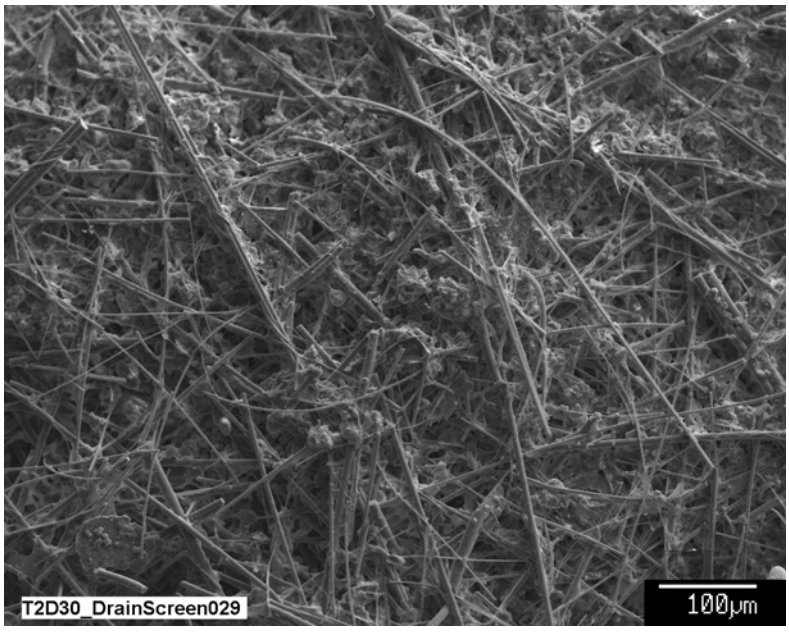

Figure 4-65. SEM image of a Test #2 Day 30 fiberglass sample on the drain collar, next to the drain screen.

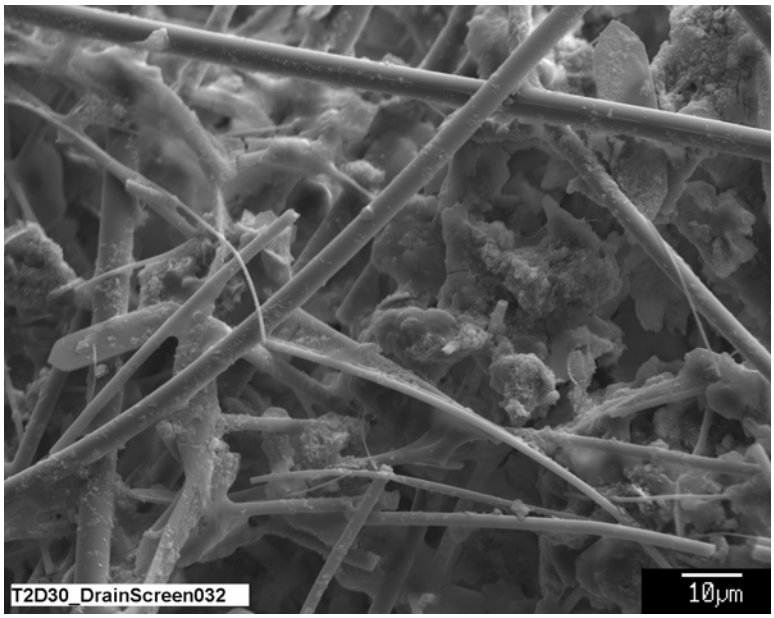

Figure 4-66. Higher-magnification SEM image of a Test #2 Day 30 fiberglass sample on the drain collar, next to the drain screen.

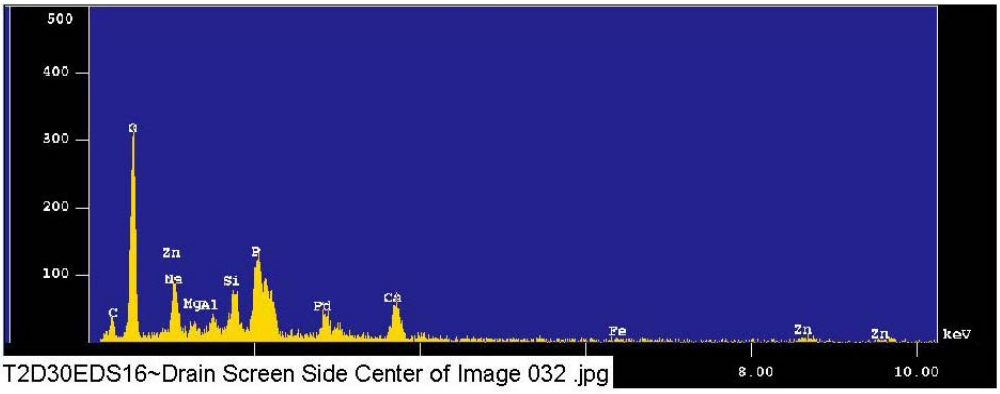

Figure 4-67. EDS counting spectrum for the center of the image shown in Figure 4-66. The deposits are composed of C, O, Na, Mg, Al, Si, P, and Ca.

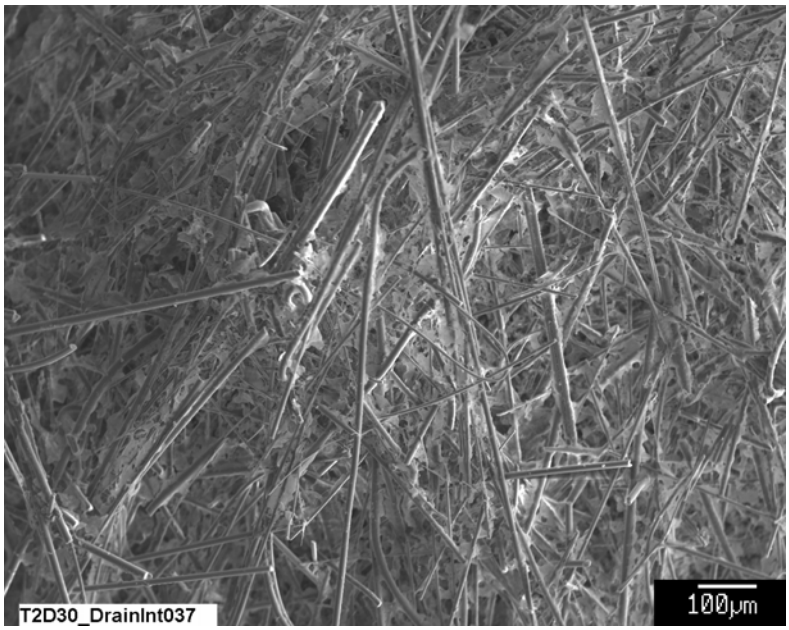

Figure 4-68. SEM image of a Test #2 Day 30 interior fiberglass sample on the drain collar. The image shows flocculence on the fiberglass.

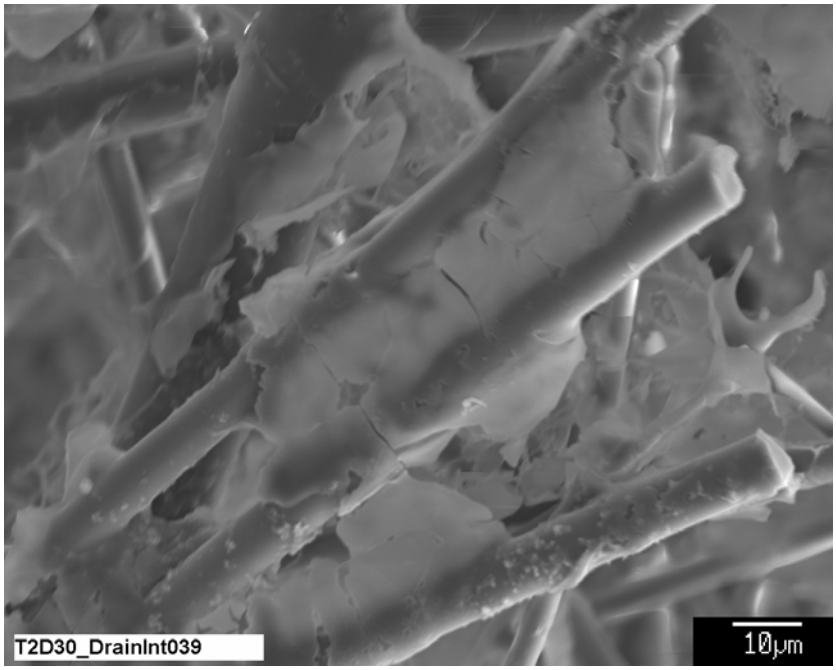

Figure 4-69. Higher-magnification SEM image of a Test #2 Day 30 interior fiberglass sample on the drain collar. The image shows flocculence or growth on the fiberglass.

Additional photos of deposits on the fiberglass test samples are presented in Appendix D.

4.4 Concrete Sample

A single concrete sample was included in the test. It is a 12-in.-square block approximately 1-1/2-in. thick, and it was submerged in the lower coupon rack (rack #1). As described in Section 4.2.1, the sample experienced a weight gain of nearly 241 g over its original weight of 7191 g. It is presumed that the bulk of that weight gain was caused by water absorption.

4.5 Solution Chemistry

4.5.1 Wet Chemistry

Wet chemistry analyses included turbidity, total suspended solids, and kinematic viscosity.

Turbidity: Figure 4-70 depicts the evolution of turbidity at 23°C and 60°C throughout the duration of the test. The first data point in the graph was taken after the latent debris and crushed concrete were added to the tank. Thus the turbidity values at this point serve as a baseline for the remainder of the test. A sharp rise in turbidity to approximately 15 NTU after 4 hours is noted. It was caused by the complete introduction of TSP chemicals at that point. The turbidity at each temperature reaches a maximum at the Day 1 test point of 20 NTU and 17.7 NTU for the 23°C and 60°C water samples, respectively. Thereafter, the turbidity values at both temperatures gradually declined to the baseline measurements. The lone exception to this overall trend occurred on the Day 3 23°C turbidity measurement. On that day, a local turbidity maximum of 14.4 NTU was measured. This was attributable to the fact that the 23°C turbidity sample on that day was immersed in the cold-water bath for a longer time than normal. Steps were taken to rigorously track the immersion time of all subsequent turbidity samples.

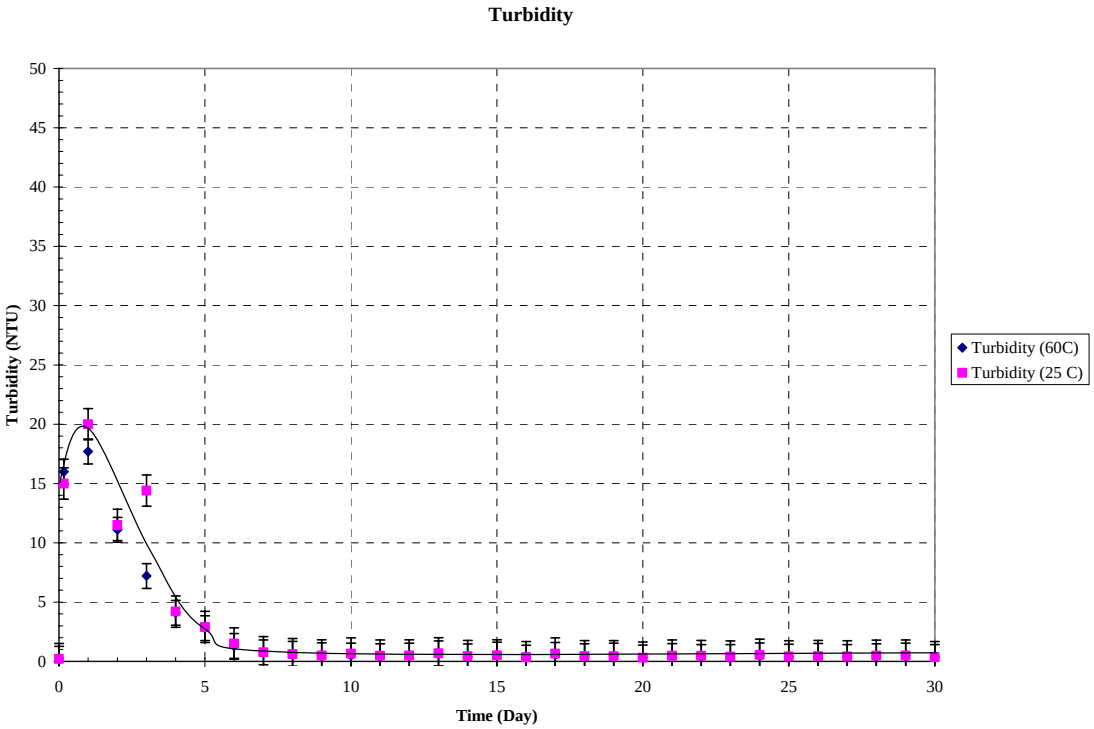

Figure 4-70. Turbidity results.

Total Suspended Solids: Total suspended solids (TSS) are measured by filtering a volume of approximately 500 mL through an in-line filter directly at the sample tap. The selected equipment ensures that TSS measurements are not affected by temperature-dependent or time-dependent precipitation reactions that may occur once the process solution is removed from the tank. The TSS concentration was 36.2 mg/L at the end of the 4-hour spray cycle. After the first 24 hours of the test, the TSS concentration dropped to 27.5 mg/L and continued to drop uniformly to approximately 10 mg/L by Day 4 of the test. The concentration remained approximately constant through the last day of testing. The TSS concentrations are shown in Figure 4-71.

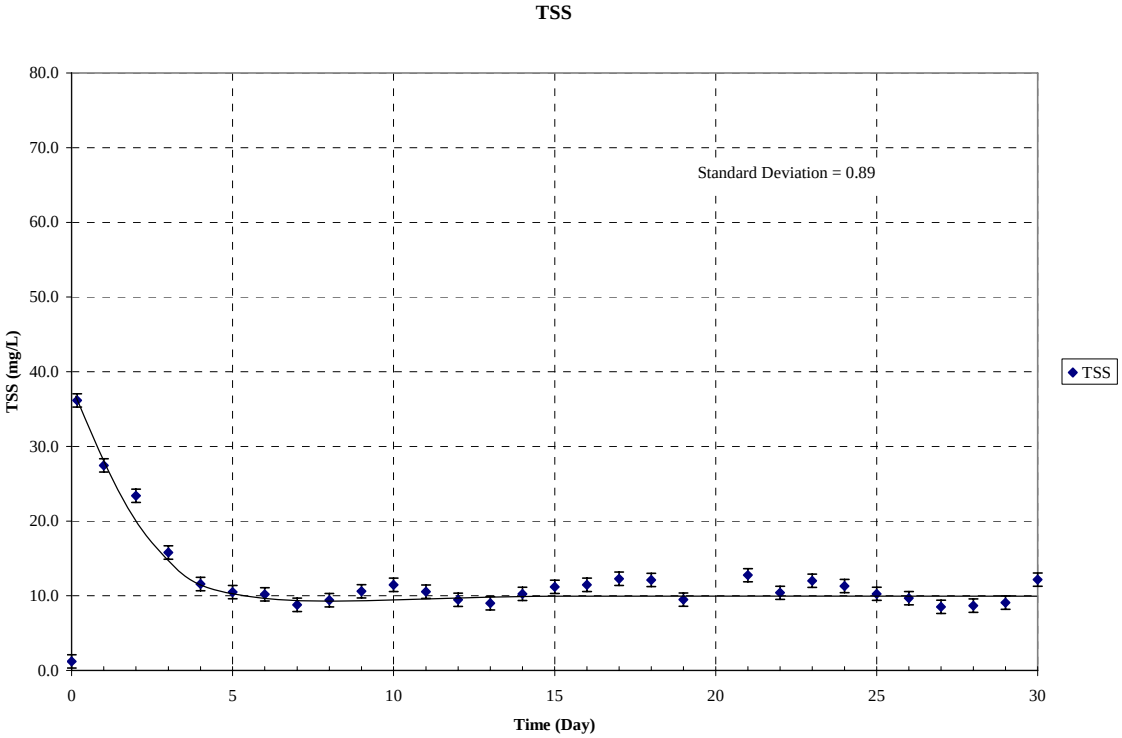

Figure 4-71. TSS results.

Kinematic Viscosity: Kinematic viscosity was measured with a Cannon-Fenske capillary viscometer. Viscosity was measured on unfiltered samples, each at a temperature of 60°C ±1.0°C (140°F ±1.8°F) and again at 23°C ± 2.0 °C (73.4°F ±3.6°F). Viscosity of water is highly sensitive to temperature, and the allowed temperature range results in a variation of viscosity of 2.9% between 59°C (138.2°F) and 61°C (141.8°F), and a 9.3% variation between 21°C (69.8°F) and 25°C (77.0°F). For this reason, temperature was measured to 0.1°C accuracy with a NIST-traceable thermometer for all viscosity measurements. Also, the measured viscosity values were corrected to a common temperature to facilitate comparisons. The corrected temperatures were 60.0°C (140°F) and 23.0°C (73.4°F). Viscosity results for Test #2 are presented in Figure 4-72. The viscosities at 60°C and 25°C remained constant throughout the test.

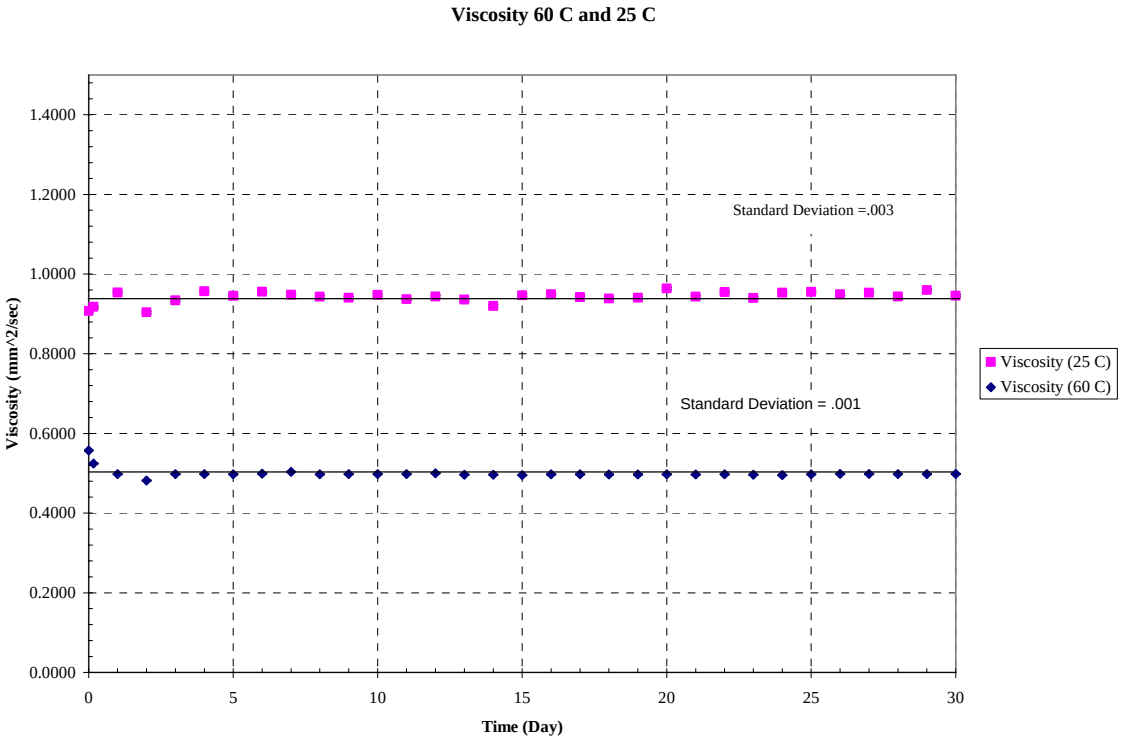

Figure 4-72. Viscosity at 60°C and 25°C.

Strain-Rate Viscosity: At Day 1 and weekly thereafter, samples were taken off-site for strain-rate viscosity measurements. All of the strain-rate viscosity measurements were performed on water samples at 60ºC and 25ºC. Figure 4-73 shows the results from each sample at 25ºC. The legend shows the dates of the samples. For example, “020605” refers to the sample from February 6, 2005. The horizontal lines of each sample indicate that the solution remained Newtonian with no significant changes throughout the 30-day test.

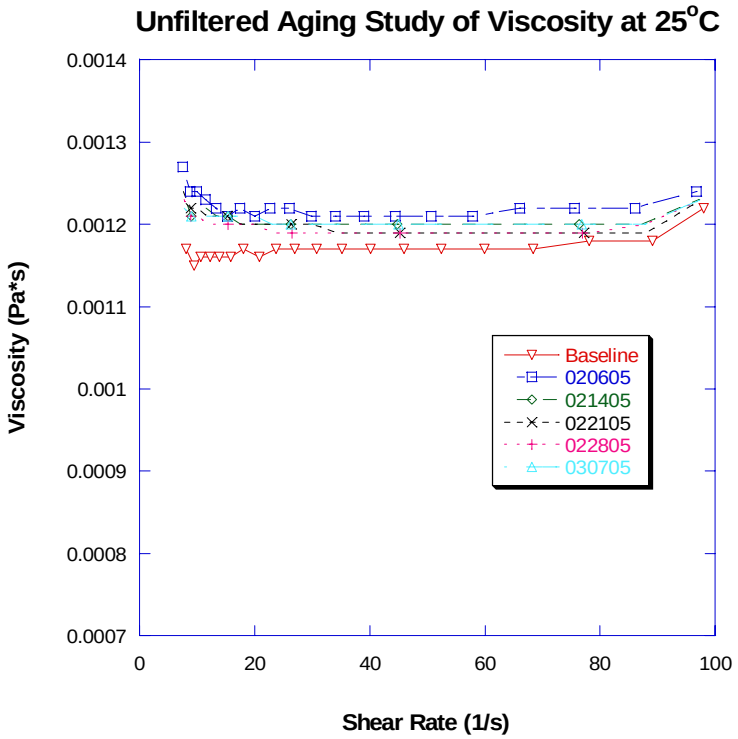

Figure 4-73. Aging study of viscosity at 25°C.

4.5.2 Metal Ion Concentration

ICP-AES results for Test #2 are contained in this section. Aluminum, copper, iron, and nickel were below detection limits and therefore are not represented graphically. The evolution of the calcium, magnesium, silica, zinc, and sodium concentrations present in the tank solution are represented in Figures 4-74 through 4-78**.** As shown in the figures, calcium (average around 8 mg/L) and sodium (average around 900 mg/L) are relatively steady throughout the test. The zinc concentration goes to zero by Day 5. Magnesium and silica show similar patterns, starting near zero and increasing to their maximum values by Day 20. The maximum value of magnesium is close to 8 mg/L, and that of silica is 90 mg/L. Measurement uncertainties are for calcium, –14% and +19%; for sodium, ±20%; for magnesium, –13% and +20%; and for silica, –9% and +12%.

In addition to elemental analyses, particulate-size distributions were measured at Day 1 and weekly thereafter. The first two days of the test showed a distribution of particulate sizes from 1 to10 microns (1%–5%) to greater than 100 microns (10%–15%). Eighty to ninety percent of the particulates were between 50 and 100 microns. The subsequent weekly samples showed a more-limited size distribution, with all particulates being in the 1– 25 micron range.

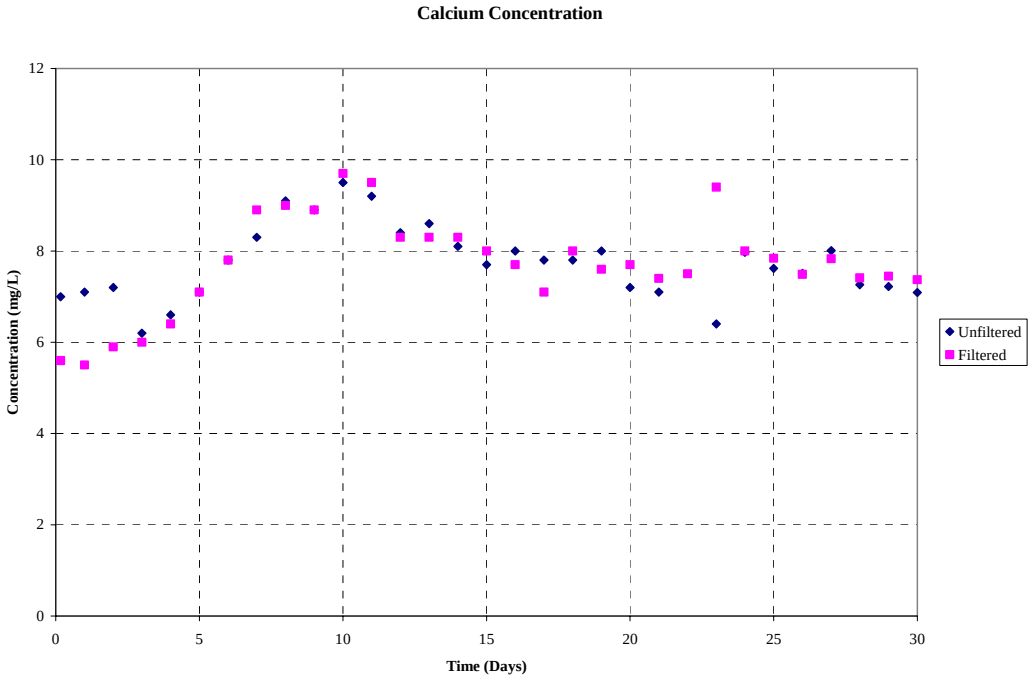

Figure 4-74. Test #2 calcium concentration.

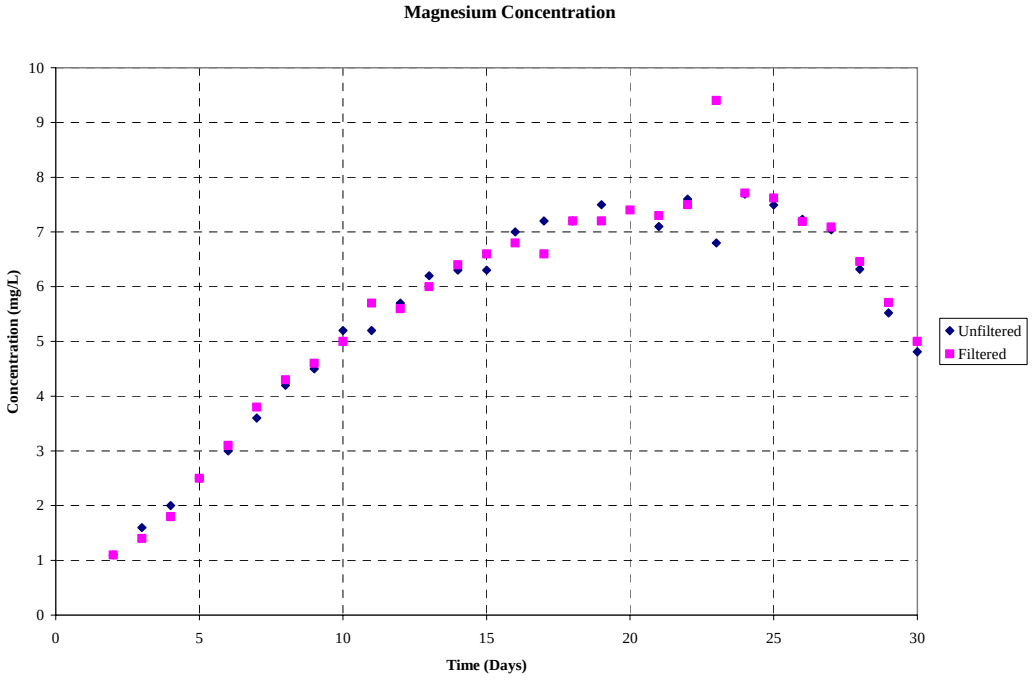

Figure 4-75. Test #2 magnesium concentration.

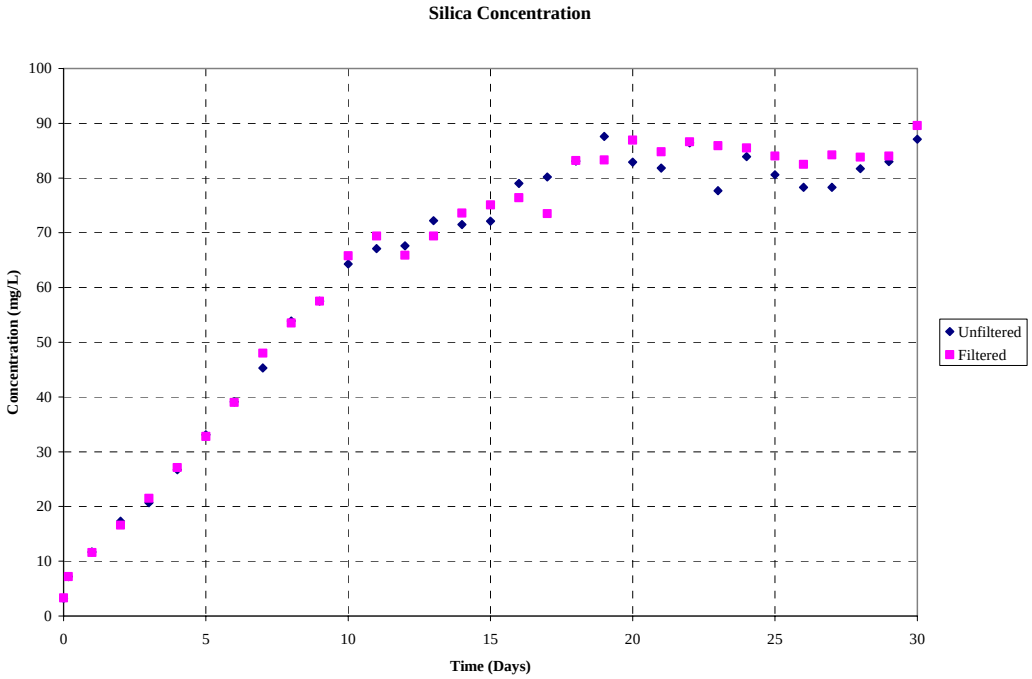

Figure 4-76. Test #2 silica concentration.

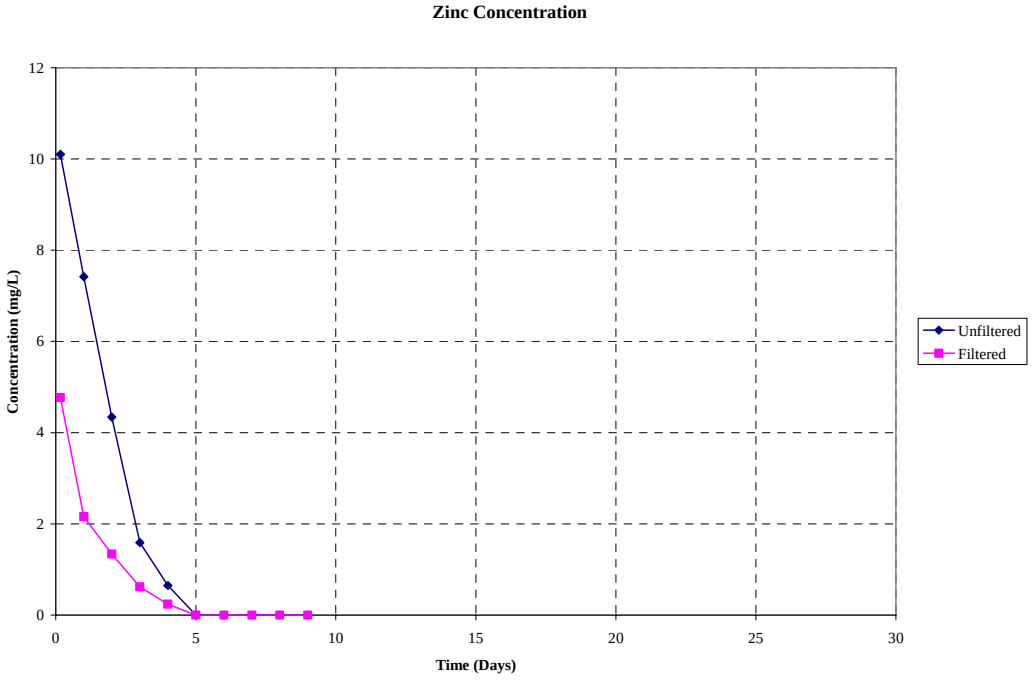

Figure 4-77. Test #2 zinc concentration.

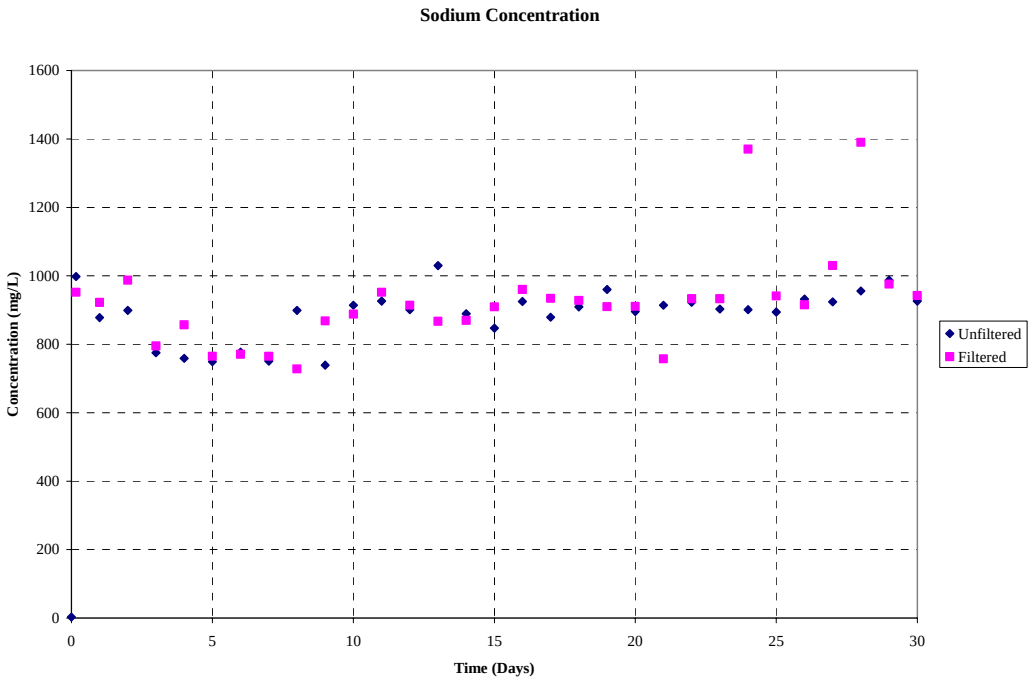

Figure 4-78. Test #2 sodium concentration.

4.5.3 General Observations

After the 4-hour spray, the water in the tank was murky and yellowish in color. After Day 1, deposits were observed on the submerged coupons. As time progressed over the first week, the water became notably clearer but was still yellow. A white deposit was also observed on the submerged (primarily galvanized) coupons, and white particles were on the bottom of the tank, the heating elements, and the fiberglass holders. Those particles may have come from the coupons.

During the second week, the water clarity significantly improved. The water was yellow, as it was in the first week. Also, white clumpy corrosion products began to appear more abundantly on the submerged fiberglass baskets and the submerged galvanized steel coupons. On the ninth day, corrosion products began to form on the copper coupons that were adjacent to the submerged galvanized steel coupons. The deposits also appeared on the submerged coated steel coupons. Throughout the second week, rust formed on the unsubmerged carbon steel coupon. About halfway through the second week, condensation on the inside of the unsubmerged view window prevented the project team from making meaningful observations of the unsubmerged coupons.

During the final two weeks of testing, no noticeable changes in tank solution or the submerged coupons were observed.

Excluding Day 30 sampling, approximately 8 gal. were removed from the system for sampling purposes. That, plus losses from evaporation and some waste, required adding 17 gal. of RO water to maintain the water volume during the course of the test.

4.5.4 Hydrogen Generation

Hydrogen remained below 0.1% during the first 10 days of testing. Figure 4-79 displays the evolution of hydrogen generation. The spike at Day 11 represents a change in the operational procedure. From the beginning of the test through Day 10, the vent valves on the tank lid were left open at all times. On Day 11 and Day 12, the vent valves were closed to determine actual hydrogen buildup without venting the tank. Through the first 10 days, the hydrogen content varied between 0.05% and 0.1%. After Day 10, the hydrogen concentration increased to 0.25% on Day 11 and then dropped to 0.15% on Day 12. This drop was probably due to the brief time when the tank vent lid was opened to return the recycled solution contents to the tank. From Day 13 on, one of the vent valves was purposely left open, which is why the hydrogen content again dropped below 0.1%.

During the third week of testing, the operational procedure for hydrogen venting returned to normal test operations and remained unchanged. After return to the normal operational procedure, the hydrogen generation remained constant.

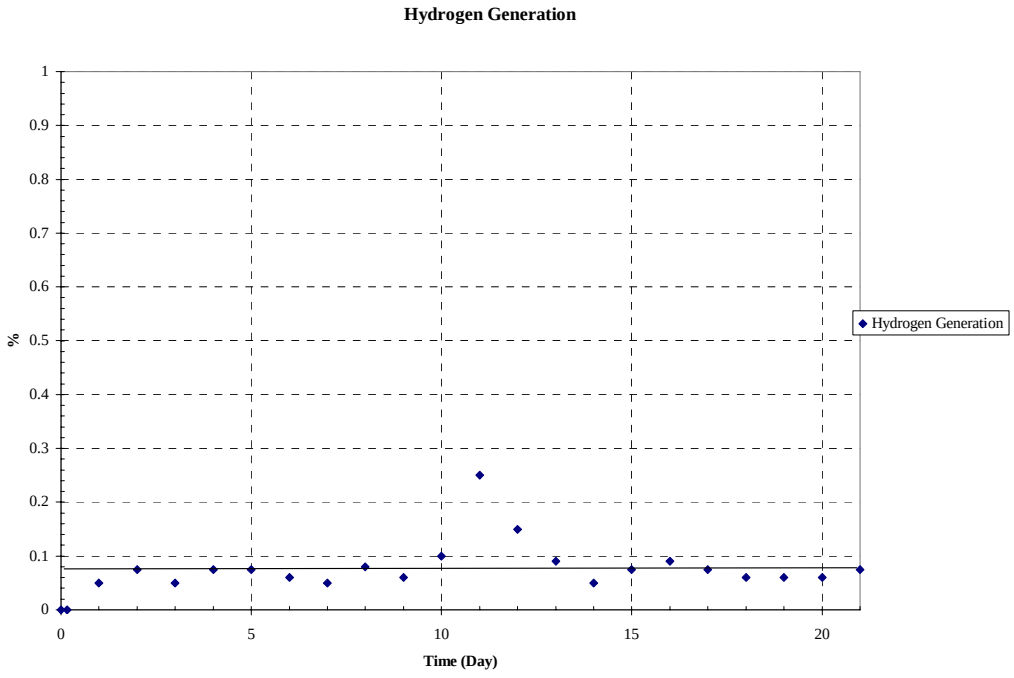

Figure 4-79. Test #2 hydrogen concentration.

4.6 Precipitated Solids

Test #2 was markedly different from Test #1 in that no precipitate was found in the test solution, even after it cooled down to room temperature. Based on a series of bench-top controlled experiments, the white precipitate observed in Test #1 contained a significant amount of aluminum. The aluminum concentration of the Test #1 solution was as high as 350 mg/L. However, the aluminum concentration of Test #2 solution was below the detection limit of ICP-AES (0.05 mg/L).

4.7 Sedimentation Analysis

Prior to ICET Test #2 initiation**,** latent debris and crushed concrete were added to the tank solution. For Test #2, this material was observed to settle completely on the bottom of the tank over the course of several days. This particulate, in combination with fugitive fiberglass strands, form the basic substrate of the sediment layer recovered from the tank at the end of Test #2. In addition, this bed may serve as a repository for chemical products that are either formed in the bed or deposited on top via settling over the course of the tests. Among all the sample types collected during ICET, tank sediment is the most heterogeneous in terms of both physical configuration and elemental composition. After draining the tank and manually recovering the sediment, 302 g was collected following Test #2. This is total mass as measured when thoroughly drained of free water by gravity but still moist. Figures 4-80 and 4-81 show an SEM image and EDS counting spectrum, respectively, of the Test #2 sediment.

Based on SEM images, the sediment sample contains particulate deposits and fiberglass debris. Due to the heterogeneous nature of the sediment, it is likely composed of corrosion products, concrete debris, dirt, and fiberglass. EDS results show that the composition of the sediment in several locations is similar to the fine powder deposited on both a vertical and a horizontal piece of the submerged rack (see Appendix B).

Qualitative visual estimates of the fiber fraction might range from 60% to 75% fiber by volume. Note that visual assessments can compare only the volume ratios and not the mass ratios. The fiber present at the bottom of the ICET tank represents fiberglass that escaped the SS mesh bags that were constructed to hold the primary volume of this debris type. In the containment pool, the sediment fiber-to-particulate ratios might vary greatly by location.

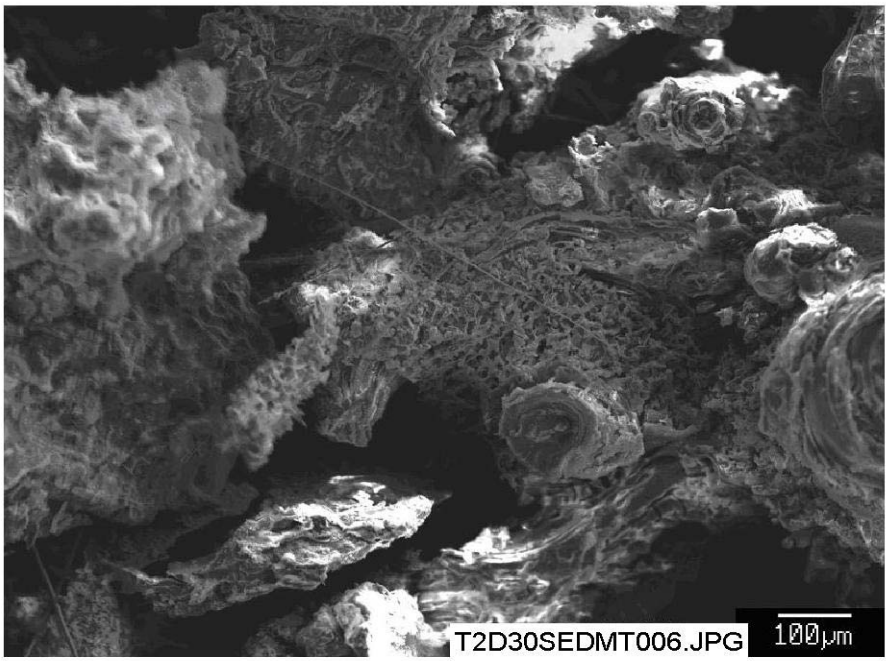

Figure 4-80. SEM image of a Test #2 Day 30 sediment sample.

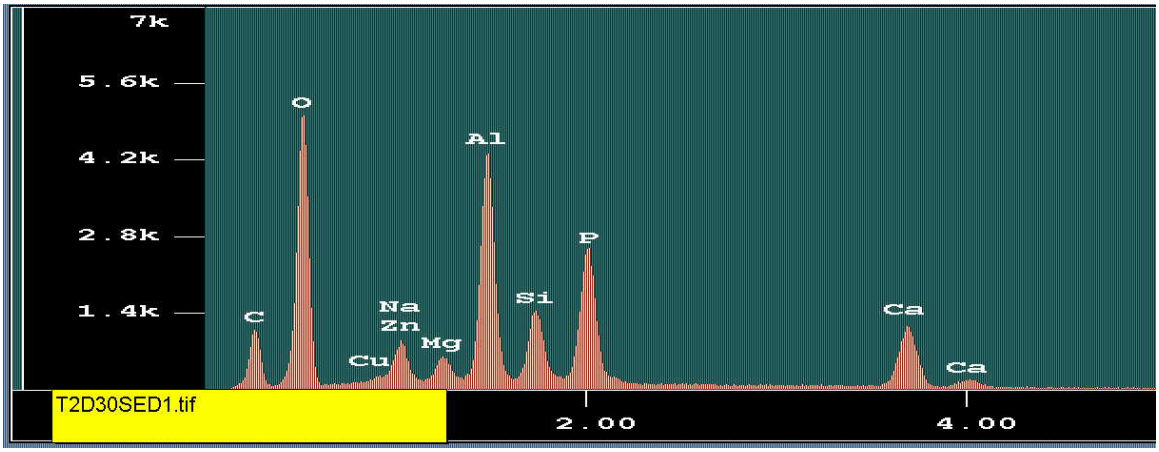

Figure 4-81. EDS counting spectrum for the circularly layered material near the right edge of Figure 4-80.

Figure 4-82 and Figure 4-83 provide a higher magnification and an additional EDS spectrum of the same Test #2 sediment shown in Figure 4-80. Underlying fibers are visible in this image, and the dominant elemental constituents are similar; however, the proportions are somewhat different. At this magnification, the spongiform deposits are

clearly seen to be different from the particulate and fibrous debris that was initially introduced into the tank. Structures of this form also permeate the fiberglass samples that have been examined for Test #2. Additional SEM and EDS results of the sediment analyses are contained in Appendix E.

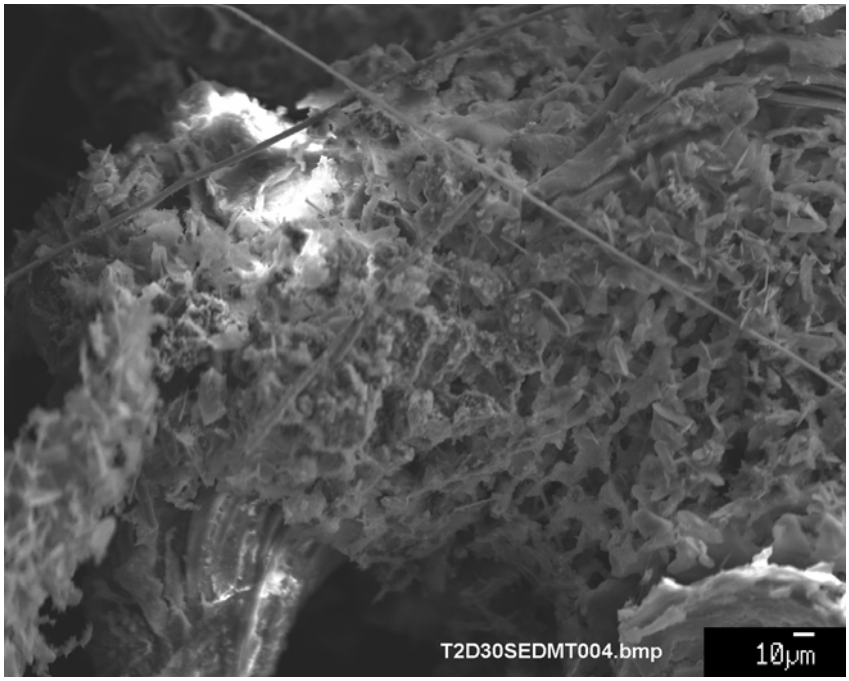

Figure 4-82. Higher-magnification SEM image of a Test #2 Day 30 sediment sample.

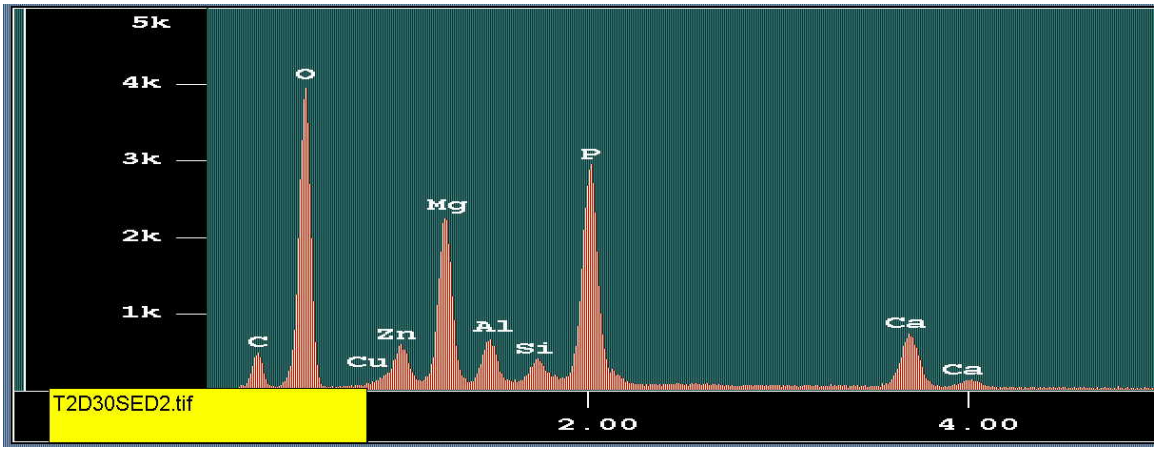

Figure 4-83. EDS counting spectrum for the porously structured material shown in Figure 4-82.

5 SUMMARY OF KEY FINDINGS

ICET Test #2 was conducted successfully, maintaining the critical physical and chemical parameters called out in the Test Plan. The test ran uninterrupted for 30 days. The solution chemistry behaved as expected with the turbidity and TSS declining from their early values to steady numbers from Day 5 until the end of the test. The kinematic viscosity was steady for the entire test; and the pH was steady, averaging a value of 7.3.

Samples of the solution were taken daily. The chemical elements present were calcium, magnesium, silica, zinc, and sodium. The silica concentration at the beginning of the test was approximately 0 mg/L, then increased nearly linearly to a value 75 mg/L by day 18 of the test. After this point, the silica concentration remained constant through the end of the test. The initial sodium concentration (after TSP injection) was approximately 900 mg/L, and it remained at that concentration for the entire test. Aluminum, copper, iron, and nickel were below detection limits. In contrast to ICET Test #1, no substantial aluminum was present in solution. Strain-rate viscosity measurements indicated that the solution remained Newtonian throughout the test. No precipitants were observed in the solution, even after it had cooled to room temperature.

The submerged aluminum and galvanized steel coupons developed significant amounts of white deposits. There was a copper layer evident on the aluminum coupons. The aluminum coupons lost an average weight of 0.9 g, while the galvanized steel coupons gained an average weight of 28.6 g. Although different in appearance, the deposits on the coated steel coupons resulted in them gaining an average weight of 3.8 g. The one uncoated steel coupon experienced a color change to reddish-brown and significant corrosion around its edges. It gained 1.4 g.

The unsubmerged coupons had random patterns that were caused by the spray. Each coupon type experienced uniform weight gains, with the coated steel gaining the most with an average weight of 1.7 g.

Deposits on the fiberglass samples increased over time, and the deposits appeared to be chemically originated for the samples not lying on the tank bottom. These deposits covered individual fiberglass strands and in some cases formed webs between strands. On most of the samples, the deposits were more prevalent on the exterior portion of the sample than on its interior. In addition to the chemical deposits, particulate deposits were observed on the exterior of those samples that were on the bottom of the tank.

Sediment on the tank bottom, that was recovered after the tank was drained, amounted to 302 g (wet). The sediment was heterogeneous in its physical composition, and it contained particulate deposits and fiberglass debris. The sediment was likely composed of corrosion products, concrete debris, dirt, and fiberglass.

REFERENCES

1. "Test Plan: Characterization of Chemical and Corrosion Effects Potentially Occurring Inside a PWR Containment Following a LOCA, Rev. 12a," October 6, 2004.

2. J. Dallman, J. Garcia, M. Klasky, B. Letellier, and K. Howe, "Integrated Chemical Effects Test Project: Test #1 Data Report," Los Alamos National Laboratory document LA-UR-05-0124, June 2005.

3. "Pre-Test Operations, Test #2," ICET-PI-012, Rev. 0, January 31, 2005.

4. "Test Operations, Test #2 (TSP at pH = 7)," ICET-PI-011, Rev. 0, January 31, 2005.

5. "Post-Test Operations, Test #2," ICET-PI-008, Rev. 2, March 7, 2005.

6. *CRC Handbook of Chemistry and Physics*, 81st ed., D. R. Lide, Ed. (CRC Press) 2000.